STUDIES ON SYNTHESIS, REACTIONS AND AND ANTIMICROBIAL ACTIVITIES OF 3-ALKYL-5-DIALKYLAMINOMETHYL PYRAZOLINES

R. A. Gadhili[a]*, A. H. Azizov[a], S. K. Zeynalova[b], Z. O. Karayev[b], A. R. Karayeva[a] and A. G. Aliyev[a]

Keywords: 3-Alkyl-5-dialkylaminomethyl pyrazolines; 3-alkyl-1-acetyl- and 1-(2-chloromethylcarbonyl)-5-(dialkylaminomethyl)-pyrazolines; 3-alkyl-5-(dialkylaminomethyl)-1-(2- phenoxyacetyl)pyrazolines; antimicrobial activity

3-Alkyl-5-dialkylaminomethyl pyrazolines, synthesized by the reaction of 1-alkyl-4-dialkylamino-but-2-en-1-ones with hydrazine hydrate, react with chloranhydride of acetic and chloroacetic acids to yield 3-alkyl-1-acetyl and 3-alkyl-5-(dialkylaminomethyl)-1-(2-chloromethylcarbonyl) pyrazolines. 3-Alkyl-1-acetyl and 3-alkyl-5-(dialkylaminomethyl)-1-(2-chloromethylcarbonyl) pyrazolines react with potassium phenolates to form 3-alkyl-5-(dialkylaminomethyl)-1-(2-phenoxyacetyl)pyrazolines. 3-Alkyl-5-dialkylaminomethyl pyrazolines and their 1-substituted derivatives show positive antimicrobial activities.

* Corresponding Authors
Fax: (+99418) 642-04-00
E-Mail: raiq.hajili@mail.ru
[a] Institute of Polymer Materials, Azerbaijan National Academy of Sciences, S.Vurgun str., 124, Az5004, Sumgait, Azerbaijan
[b] Azerbaijan Medical University, Bakykhanov str.,23, AZ0022, Baku, Azerbaijan

Introduction

The pyrazolines show anti-inflammatory, antipyretic, anticonvulsive, anti-tuberculous and other physiological activities[1-3] and find wide applications in medicine as a drug, such as analgin, amidopyrine, butadione, etc.[4] It is known that an interaction of 2-chlorvinyl ketones with alkyl hydrazines leads to the formation of 1,3-dialkylpyrazolines,[5] and of 3,4-bis(dimethyamine)but-2-en-1-ones with hydrazine hydrate to the formation of 3-R-5-dimethylaminomethyl pyrazoles.[6] Further, the reaction of 1-(2-furyl)-3-aryl-2-propen-1-ones with hydrazine and its derivatives leads to 3-(2-furyl)-5-arylpyrazolines.[7]

The aim of this work is synthesize new pyrazoline derivatives by the reactions of 4-diethylamine(morpholine)but-2-en-1-ones (**1, 2a, b**) with hydrazine hydrate. The starting compounds (**1, 2a, b**) were prepared by known procedure of interaction of -chlorbutyl-2-en-1-ones with secondary amines.[8] The physical-chemical constants of ketones (**1, 2a, b)** are identical with such ones listed in the literature.[8]

Results and Discussion

It was observed that the reaction of alkyl-4-diethylamine(morpholine)but-2-en-1-ones with hydrazine hydrate in ether at 35-40 °C for 6 h leads to the formation of 3-alkyl-5-diethylamine(morpholine)methyl pyrazolines (**3, 4a, b**) with yields of 68-75 %. The pyrazolines (**3, 4a, b**) contain highly mobile hydrogens which are easily acylated with acyl chlorides. It was observed that a reaction of pyrazolines (**3, 4a, b**) with acylchlorides in the presence of the equimolar quantities of triethyleamine (for binding of isolated HCl) in anhydrous ether at 10-15 °C for 4 h leads to the formation of 3-alkyl-1-acetyl-5-diethylamine (morpholine)methyl pyrazolines (**5, 6a, b**) in yields of 64-70 %. However, reaction with monochloroacetyl chloride acid at 20-25 °C for 5 h leads to the formation of 3-alkyl-1-(2-chlormethylcarbonyl)-5-diethylamine (morpholine) methyl pyrazolines (**7, 8a, b**) with yields of 63-67 %.

The synthesized pyrazolines (**7, 8a, b**) contain a reactive chlorine atom, which can be easily substituted by potassium phenolates. Thus it was observed that the reactions of (**7, 8a, b**) with potassium phenolates in aqueous-benzene medium at 65-70 °C for 6 h leads to the formation of 3-alkyl-5-diethylamine(morpholine)methyl-1-(2-phenoxymethyl-carbonyl)pyrazolines (**9, 10a, b**) in yields of 66-70 %.

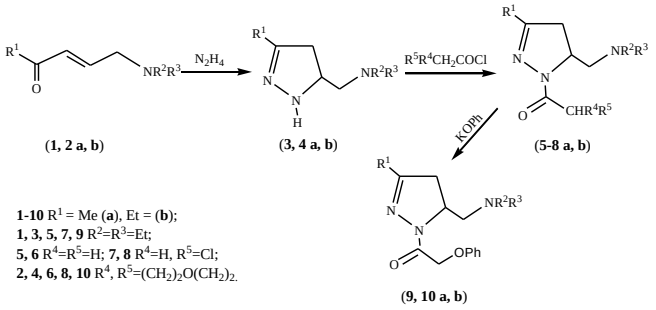

Scheme1. Synthesis of 3-alkyl-5- diethylamine(morpholine) methyl-1-(2-phenoxymethyl-carbonyl)pyrazolines

The structure of pyrazolines derivatives (**3-10 a, b**) has been established on the basis of data of the elemental analysis, IR and ^{1}HNMR spectra. In the IR-spectra of pyrazolines (**3, 4a, b**) there are the absorption bands of NH fragment in the region of 3300-3324 cm^{-1}, which disappear in the spectra of pyrazolines (**5-8 a, b**). In (**5-8 a, b**), the characteristic[9] signal of carbonyl group in the region of 1700-1725 cm^{-1} appears. In the IR-spectra of (**9, 10 a, b**) besides absorption bands of C=O group, the absorption band of C-Cl bond in the region of 708-732 cm^{-1} is observed. In

the ^{1}HNMR spectra of pyrazolines (**3, 4 a, b**), the signals of N-H protons (δ ppm: 5.70-6.15) are obtained, which disappear in the spectra of pyrazolines (**5-10 a, b**). In the spectra of pyrazolines (**5 a, b**), signals of $COCH_3$ (δ 2.20-2.30) were observed. Similarly, pyrazolines (**6 a, b**) showed signals for $COCH_2Cl$ at δ = 3.75-4.05. The overlapped signals $2CH_2$, $N(C\underline{H_2}CH_3)_2$ groups, CH_2N and CH_2 of pyrazoline nuclei were observed at δ = 2.20-3.10. The signals of $N(CH_2)_2$, $N(CH_2)_2(CH_2)_2O$ group, CH_2N and CH_2 of pyrazoline nuclei are seen δ = 2.15-3.36.

Experimental

Chemical part

The IR-spectra have been recorded on Fourier-spectrometer Protege-460 Nikolet from thin layer. The ^{1}H NMR spectra were recorded on Tesla BS-567 spectrometer (100 MHz), internal standard HDMS (0.05 ppm), solvents: CCl_4 (**3-6**) and DMSO-d_6 for others. The purity of the synthesized compounds was checked by TLC on the plates Silufol UV-254.

3-Alkyl-5-diethylamino(morpholine)methyl pyrazolines (3,4 a, b)

To a solution of 50 mmol 1-alkyl-4-diethylamino-(morpholine)but-2-en-1-ones (**1, 2 a, b**) in 30 ml of ethanol added dropwise 2.2 ml (50 mmol) hydrazine hydrate at 20-25 °C. The reactants were mixed at 50-55 °C for 5 h. After cooling the solvent was distilled off, and the residue was sublimed in vacuum.

5-Diethyl-3-methylaminomethylpyrazoline (3a)

Yield 75%, b.p. 89-91 °C (3 mm Hg). n_D^{20} 1.4731, d_4^{20} 0.9378. IR: 3316 (NH), 2950 ($CH_{pyrazoline}$), 1525 (C=N) cm^{-1}. ^{1}H NMR δ =1.30 (t, 3H, CH_2CH_3), 2.10 (s, 3H, CCH_3), 2.25-2.87 [m, 2H, (CH_2, H-4), (2H, CH_2CH_3), 2H, NCH_2], 3.46 m (m, 1H, CH, H-5), 5.75 (s,1H, NH). Anal. Calcd for $C_9H_{18}N_3$: C 64.28; H 10.72; N 25.00. Found: C 63.51; H 9.82; N 25.47.

5-Diethyl-3-ethylaminomethylpyrazoline (3b)

Yield 73%, b.p. 96-98 °C (1 mm Hg). n_D^{20} 1.4722, d_4^{20} 0.9153. IR: 3324 (NH), 3000 ($CH_{pyrazoline}$), 1534 (C=N) cm^{-1}. Anal. Calcd for $C_{10}H_{20}N_3$: C 65.93; H 10.91; N 23.08. Found: C 65.29; H 10.53; N 23.59.

5-Morpholinomethyl-3-methylpyrazoline (4a)

Yield 71%, b.p. 118-120 °C (4 mm Hg). n_D^{20} 1.5170, d_4^{20} 0.0939. IR: 3340 (NH), 2940 ($CH_{pyrazoline}$), 1520 (C=N), 1245, 1194 (C-O) cm^{-1}. ^{1}H NMR δ = 2.15 (s, 3H, CCH_3), 2.2-3.36 (m, 2H, (CH_2, H-4), 4H, $(CH_2)_2N$, 2H, NCH_2), 3.54 (t , 2H, $(CH_2)_2O$), 4.20 m [1H, (CH, H-5)], 5.90 (s, 1H, NH). Anal. Calcd for $C_9H_{16}N_3O$%: C 59.34; H 8.79; N 23.08. Found: C 59.70; H 8.34; N 23.48.

5-Morpholinomethyl-3-methylpyrazoline (4b)

Yield 68%, b.p. 126-127 °C (3 mm Hg). n_D^{20} 1.5138, d_4^{20} 1.0064. IR: 3312 (NH), 2930 ($CH_{pyrazoline}$), 1573 (C= N), 1230, 1197 (C-O) cm^{-1}. Anal. Calcd for $C_{10}H_{18}N_3O$: C 61.23; H 9.18; N 21.43. Found: C 61.75; H 9.53; N 21.70.

3-Alkyl-1-acetyl-5-diethylamino(morpholine)methylpyrazolines (5,6a,b)

To a solution of 25 mmol pyrazoline (**3, 4 a, b**) in 50 ml of anhydrous ether, 2 g (25 mmol) of acetyl chloride and 3.5 ml (25 mmol) of triethyl amine was added dropwise at 0-5 °C. Then the reactants were mixed for 5 h at 15-20 °C temperature. It was washed by 2 % aqueous solution (50 ml) of sodium bicarbonate, ether layer was separated, the aqueous layer was treated by 40 ml ether and the combined ethereal extracts were dried over $MgSO_4$. After distillation of solvent the residue was sublimed in vacuum.

1-Acetyl-5-(diethylaminomethyl)-3-methylpyrazoline (5a)

Yield 70 %, b.p. 129-130 °C (5 mm Hg). n_D^{20} 1.4836, d_4^{20} 0.9871. IR: 2970 ($CH_{pyrazolin}$), 1720 (C=O), 1440 (C=N) cm^{-1}. ^{1}H NMR δ = 0.95 (t , 3H, CH_2CH_3), 2.00 (s ,3H, CCH_3), 2.13 (s , 3H, $COCH_3$), 2.20-2.89 (m , 2H, (CH_2, H-4), (2H, CH_2CH_3), 2H, NCH_2), 4.37 (m , 1H, CH, H-5). Anal. Calcd for $C_{11}H_{20}N_3O$: C 62.86; H 9.52; N 20.00. Found: C 62.53; H 9.79; N 20.35.

1-Acetyl-5-(diethylaminomethyl)-3-methylpyrazoline (5b)

Yield 67 %, b.p. 130-132 °C (2 mm Hg). n_D^{20} 1.4824, d_4^{20} 0.9740. IR: 2895 $CH_{pyrazoline}$), 1722 (C=O), 1523, 1505 (C= N) cm^{-1}. Anal Calcd for $C_{11}H_{20}N_3O$: C 64.29; H 9.82; N 18.75. Found: C 64.98; H 9.17; N 18.31.

1-Acetyl-5-(morpholinomethyl)-3-methylpyrazoline (6a)

Yield 68 %, b.p. 150-152 °C (4 mm Hg). n_D^{20} 1.5274, d_4^{20} 1.0058. IR: 3005, 2980 ($CH_{pyrazoline}$), 1724 (C=O), 1517 (C=N), 1220, 1204, 1162 (C-O) cm^{-1}. Anal Calcd for $C_{11}H_{19}N_3O_2$: C 58.66; H 8.44; N 18.66. Found: C 58.09; H 8.56; N 18.21.

1-Acetyl-5-(morpholinomethyl)-3-ethylpyrazoline (6b)

Yield 64 %, b.p. 166-168 °C (4 mm Hg). n_D^{20} 1.5232, d_4^{20} 0.9853. IR: 3000 ($CH_{pyrazoline}$), 1725 (C=O), 1520 (C=N), 1205, 1150 (C-O) cm^{-1}. Anal. Calcd for $C_{12}H_{21}N_3O$: C 60.25; H 8.78; N 17.57. Found: C 59.38; H 8.52; N 17.33.

3-Alkyl-5-diethylamine(morpholine)methyl-1-(chloracetyl)-pyrazolines (7, 8 a, b)

2.8 g (25 mmol) of monochloroacteyl chloride was added drop wise to a solution of 25 mmol pyrazoline (**3, 4 a, b**) and 3.5 ml (25 mmol) triethyl amine in 50 ml of anhydrous ether at 0-5 °C. The reaction mixture was stirred for 6 h at 25-30 °C. The follow up was similar to the procedure adopted for the synthesis of the compounds (**5, 6 a, b**).

5-(Diethylaminomethyl)-3-methyl-1-(chloracetyl)pyrazoline (7a)

Yield 67 %, b.p. 160-162 °C (3 mm Hg). n_D^{20} 1.4950, d_4^{20} 1.0431. IR: 2897 ($CH_{pyrazoline}$), 1715 (C=O), 1440, 1456 (C=N), 720 (CCl) cm^{-1}. ^1H NMR δ = 0.91 (t, 3H, CH_2CH_3), 2.10 (s , 3H, CCH_3), 2.27-3.05 (m, 2H, (CH_2, H-4), (2H, CH_2CH_3), 2H, NCH_2), 4.00 (s , 2H, CH_2Cl), 4.12-4.53 (m, 1H, H-5). Anal. Calcd for $C_{11}H_{20}ClN_3O$: C 53.77; H 8.15; N 17.11. Found: C 54.63; H 8.02; N 17.48.

5-(Diethylaminomethyl)-3-ethyl-1-(chloracetyl)pyrazoline (7b)

Yield 65 %, b.p. 170-172 °C (3 mm Hg). n_D^{20} 1.4920, d_4^{20} 1.0267. IR: 2945 ($CH_{pyrazoline}$), 1717 (C=O), 1490, 1475 (C=N), 708 (CCl) cm^{-1}. Anal. Calcd for $C_{12}H_{22}ClN_3O$: C 55.49; H 8.49; N 16.18. Found: C 56.10; H 8.29; N 16.76.

5-(Morpholinomethyl)-3-methyl-1-(chloracetyl)pyrazoline (8a)

Yield 65 %, b.p. 184-185 °C (3 mm Hg). n_D^{20} 1.5095, d_4^{20} 0.9847. IR: 3010 ($CH_{pyrazoline}$), 1708 (C=O), 1515, 1480 (C=N), 1235, 1210, 1196 (C-O), 732 (CCl) cm^{-1}. ^1H NMR δ = 2.00 (s, 3H, CCH_3), 2.15-3.10 (m, 2H, (CH_2, H-4), (4H, $N(CH_2)_2$), 2H, CH_2N), 3.75 (s, 2H, CH_2Cl), 4.10-4.52 (s, 1H, H-5). Anal. Calcd for $C_{11}H_{18}ClN_3O_2$: C 50.87; H 6.94; N 16.18. Found: C 51.64; H 7.16; N 16.59.

5-((Morpholinomethyl)-3-ethyl-1-(chloracetyl)pyrazoline (8b)

Yield 63 %, b.p. 201-203 °C (2 mm Hg). n_D^{20} 1.5068, viscous liquid. IR: 2976 ($CH_{pyrazoline}$), 1722 (C=O), 1455 (C=N), 1200, 1192 (C-O), 715 (CCl) cm^{-1}. Anal. Calcd for $C_{12}H_{20}ClN_3O_2$: C 52.65; H 7.31; N 15.36. Found: C 51.88; H 7.52; N 15.54.

3-Alkyl-5-(dialkylaminomethyl)-1-(2-phenoxyacetyl)pyrazolines (9, 10 a, b)

A solution of KOH in water (50 mL) was added drop wise to 1.9 g (20 mmol) of phenol, then 20 mmol of compound (**5, 6 a, b**) dissolved in 50 ml benzene was added. The reaction mixture was heated at 65-70 °C for 6 h. After cooling it was washed with 2 % aqueous solution (40 ml) of sodium bicarbonate, benzene layer was separated, aqueous layer was treated by 40 ml of ether, the combined organic extracts were dried over $MgSO_4$. After distillation of solvents the residue was sublimed in vacuum.

5-(Diethylaminomethyl)-3-methyl-1-(2-phenoxyacetyl)pyrazolines (9a)

Yield 70 %, b.p. 189-191 °C (2 mm Hg). n_D^{20} 1.5340, d_4^{20} 1.0214. IR: 3100, 3065 (CH_{arom}), 2905 ($CH_{pyrazoline}$), 1715 (C=O), 1620, 1455 (C=C, C=N) cm^{-1}. ^1H NMR δ = 1.10 (t, 3H, CH_2CH_3), 2.08 (s, 3H, CCH_3), 2.20-3.00 (m, 2H, (CH_2, H-4), (4H, $N(CH_2)_2$), 2H, CH_2N), 3.62 (c, 2H, CH_2Ph), 4.17-4.55 (m, 1H, H-5). Anal. Calcd for $C_{17}H_{25}N_3O_2$: C 67.33; H 8.25; N 13.86. Found: C 68.11; H 8.07; N 14.12.

5-(Diethylaminomethyl)-3-ethyl-1-(2-phenoxyacetyl)pyrazoline (9b)

Yield 65 %, b.p. 202-203 °C (1 mm Hg). n_D^{20} 1.5264, d_4^{20} 1.0013. IR: 3115, 3034 ($CH_{arom.}$), 2923 ($CH_{pyrazoline}$), 1720 (C=O), 1635, 1607, 1450 (C=C, C=N) cm^{-1}. Anal. Calcd for $C_{18}H_{27}N_3O_2$: C 68.14; H 8.52; N 13.25. Found: C 67.48; H 8.37; N 13.52.

5-(Morpholinomethyl)-3-methyl-1-(2-phenoxyacetyl)pyrazoline (10a)

Yield 67 %, b.p. 227-229 °C (2 mm Hg). n_D^{20} 1.5470, viscous liquid. IR: 3140, 3054 ($CH_{arom.}$), 2935, ($CH_{pyrazoline}$), 1705 (C=O), 1615, 1590, 1470 (C=C, C=N) cm^{-1}. ^1H NMR δ = 2.00 (s, 3H, CCH_3), 2.28-3.30 (m, 2H, (CH_2, H-4), ((4H, $N(CH_2)_2$), 2H, CH_2N, 3.68 (s, 2H, CH_2Cl), 4.00-4.48 (m, 1H, H-5). Anal. Calcd for $C_{17}H_{23}N_3O_3$: C 64.35; H 7.25; N 13.25. Found: C 64.96; H 7.40; N 13.02.

5-(Morpholinomethyl)-1-(2-phenoxyacetyl)-3-ethylpyrrazoline (10b)

Yield 66 %, b.p. 230-231 °C (2 mm Hg). n_D^{20} 1.5426, viscous liquid. IR: 3055, 3020 ($CH_{arom.}$), 2980 ($CH_{pyrazoline}$), 1718 (C=O), 1648, 1620, 1427 (C=C, C=N) cm^{-1}. Anal. Calcd for $C_{18}H_{25}N_3O_3$: C 65.26; H 7.55; N 12.69. Found: C 64.93; H 7.81; N 12.47.

Biological part

The antimicrobial activities of 3-alkyl-5-diethylaminomethylpyrazolines (**3 a, b**), 3-alkyl-1-acetyl-5-(diethylaminomethyl)pyrazolines (**5 a ,b**) and 3-alkyl-5-(diethylaminomethyl)-1-(chloracetyl)pyrazolines (**7 a, b**) were investigated by a method of serial consecutive breeding in a sterile distilled water in relation to grampositive bacteria *S. aureus 209*, gramnegative bacteria *P. aeruginosa 40*, *E. coli M17*, and from fungi *C.albicans 23*. The breeding was begun with 500 mcg mL^{-1} depending on activities of the compounds. The obtained data are presented in Table 1.

Table 1. Antimicrobial activities of the compounds (**3**), (**5**) and (**7**) (MSC mcg mL^{-1})

Compound	*S.aureus* 209	*P.aerugi-nosa* 40	*E. coli* M-17	*C.albicans* 23
3a	62.5	62.5	125	31.2
3b	62.5	62.5	125	31.2
5a	125	125	250	62.5
5b	125	125	250	62.5
7a	31.5	62.5	62.5	15.6
7b	31.5	62.5	125	15.6

It is observed that the compounds (**3, 5, 7**) show a significant antimicrobial activity against bacteria *S. aureus 209* and *C .albicans 23*. The compounds (**7 a, b**) containing chlorine atom in position 1, show higher antimicrobial activity to all cultures in comparison with (**3, 5 a, b**).

 DOI: 10.17628/ecb.2015.4.535-538

Thus, it has been found that the substituents in molecules of pyrazolines (**3, 5** and **7**) in position 1 affect the antimicrobial activity in the following order: Cl > H > CH_3.

Conclusion

The previously non-described 5-dialkylaminomethyl pyrazoles have been synthesized. These can be used as initial syntones for preparation of the structural analogs of molecules used in medicine, e.g. amidopyrine, analgin, antipyrine, etc.

References

[1]Khudina, O. G., Burgart, Ya. V., Saloutin, V. I., Kravchenko, M.A., *Zh. Org. Khim.*, **2011**, *47*, 887.

[2]Khloya, P., Kumar, P., Mittal, A., Aggarwal, N. K., Sharma, P. K., *Org. Med. Chem. Lett.* **2013**. *3*, 9.

[3]Pawar, R. B., Mulwad, V. V., *Chem. Heterocyclic Compd*., **2004**, *40*, 219.

[4]Mashkovski, M. D., *Drug means. M.: Novaya volna*, **2002**, *1*, 449.

[5]Bozhenkov, G. V., Savosik, V. A., Larina, L. I., Klyba, L. V., Zhanchipova, E. P., Mirskova, A. N., Levkovskaya, G. G., *Zh. Org. Khim.*, **2008**, *44*, 1024.

[6]Hajili, R. A., Dikusar, E. A., Aliev, A. G., Karayeva, A. R., Nagiyeva, Sh. F., Potkin, V. I., *Zh. Org. Khim.*, **2015**, *51*, 547.

[7]Zühal Özdemir, Z., Burak Kandilci, H., Bülent Gümüşel, Ünsal Çalış, Altan Bilgin, A., *Eur. J. Med. Chem.*, **2007**, *42*, 373.

[8]Ibrahimov, I. I., Mamedov, E. I., Aliyev, A. G., Mehdiyeva, T. S., Guseinov, S. A., Mehtiyeva, Sh. E., Mamedov, N. N., *Zh. Org. Khim.*, **1990**, *26*, 2294.

[9]Gordon, A., Ford, R., *Sputnik Khimika, Moskva, Mir*, **1976**, 203.

Received: 05.11.2015.
Accepted: 12.01.2016.

ADENOSINE DEAMINASE AND ITS ISOENZYMES IN ASCITES WITH DIFFERENT ETIOLOGIES

Mohamed Ahmed Abdelmoaty[*a] andAhmed Mohamed Bogdady[b]

Keywords: ADA; tuberculosis; liver cirrhosis

Adenosine deaminase (ADA) activity increased in certain clinical conditions including tuberculosis and bacterial infections. In this study, the ADA isoenzymes patterns are assayed in ascites of different etiologies. Ninety two patients with ascites were selected and investigated to determine the cause of ascites. Total ADA and its isoenzymes are assayed spectophotometerically beside polyacrylamide gel electrophoretically. The total ADA in ascitic fluid secondary to parainfection in case of TB, abdominal cancer and liver cirrhosis is found to be 34.5±11.1, 87.6±23.6, 32.7±10.1 and 28.5±7.3 U L^{-1} respectivly. The ADA1m was 24.5±11.1, 4.3±1.9, 2.8±2.2 and 10.1±3.3 U L^{-1}. ADA1c was 7.8±3, 16.5±6.2, 4.7±1.3 and 10.1± .3 U L^{-1} respectivly. ADA2 was 2.2±3.9, 65.9±33.5, 26.2±6.2 and 3.3±9.7 U L^{-1} respectively. Hence it is concluded that total ADA above 41 U L^{-1} and ADA2 above 32 U L^{-1} in ascetic fluid have high sensitivity value in TB peritonitis. The ascitic fluid ADA1m/ADA more than 50 % has high specificty value in parainfective peritonitis. Total ascitic ADA<41 U L^{-1} and ADA2/ADA ratio >50 % have high specificity in abdominal cancer.

* Corresponding Authors
Fax: Tel; 002- 01226388153
E-Mail: abdelmoaty5@yahoo.com
[a] Medical Biochemistry department Sohag Faculty of Medicine, Sohag University Egypt.
[b] Departments of Internal Medicine, Faculty of Medicine, Sohag University.

Introduction

The ascite is an accumulation of fluid in the abdominal cavity. The two main ascites are transudate (total protein < 30 g L^{-1}) which is caused by liver cirrhosis (LC), and exudate (total protein > 30 g L^{-1}) which is caused by tuberculous peritonitis (TBP) and abdominal cancer (AC) respectively in Egypt.[1] TBP and AC require rapid recognition for the appropriate therapeutic management.[2] Clinically, etiological diagnosis of ascites is very difficult especially in exudative type because of the lack of specific differential clinical, radiological, or laboratory findings. Peritoneoscopy is the method of choice in the diagnosis of the cause of ascites.[3] However, the diagnostic failure rate of peritoneoscopy can reach as high as approximately 14 %; the main reason for failure is the interference from adhesions due to tumor, tuberculosis or previous surgery.[4]

Adenosine deaminase enzyme (adenosine amino hydrolase, EC 3.5.4.4. ADA) catalyzes the deamination of adenosine and deoxyadenosine to inosine and deoxyinosine respectively. It is widely distributed in human tissues. ADA is critical in the development and function of immune system.[5,6] Clinical interest concering ADA enzyme has been reviewed due to the association between combined immunodeficiency and ADA deficiency.[5,6] ADA helps in proliferation and differentiation of lymphocytes especially T lymphocytes,[7] and is a significant indicator of active cellular immunity.[8] Thus, ADA has been proposed to be a useful surrogate marker for the diagnosis of tuberculosis (TB) because it can be detected in body fluids such as pleural,[5] pericardial,[9] cerebrospinal fluid,[10] and peritoneal fluid,[11] and elevated ADA levels have been reported in these cases.

Two isoenzymes of ADA, namely ADA1 and ADA2, have unique biochemical properties.[12] ADA1m isoenzyme is found as a monomer but ADA1c is a dimer.[13] The ADA1 isoenzyme is found in all cells, with the highest activity in lymphocytes and monocytes, whereas ADA2 isoenzyme is found only in monocytes.[14] The assay of ADA activity in ascites may be very useful in detecting the etiology of ascites, especially in the case of tuberculosis, which is characterized by an increase in activity.[15]

The purpose of this study is to evaluate the benefit of using peritoneal fluid ADA and its isoenzymes to clarify the final etiology of ascites.

Patients and methods

Study subject

Ninety-two patients, suffering from ascites with different etiology and had undergone abdominal ultrasonography and abdominal computed tomography (CT) scan with or without peritoneoscopy for diagnosis, were enrolled in this study. The study was carried out in Sohag Faculty of Medicine Hospital from January to July 2014.

All patients had laboratory tests such as complete blood count, serum liver function tests (albumin, bilirubin, AST, ALT and alkaline phosphatse), ascetic fluid albumin and Carcinoembryonic antigen (CEA) as tumor marker, cytology of ascetic fluid and ascetic fluid ADA. TBP was diagnosed on the basis of one of the following criteria: (1) ascetic fluid showed positive acid-fast bacilli stain and culture; (2) tuberculosis polymerase chain reaction test from ascites specimen was positive or (3) caseating granuloma was noted in the peritoneal biopsy specimen.

Abdominal cancer was diagnosed if cancer cells from ascetic fluid cytology were detected or cancer cells were documented from the peritoneoscopic biopsy specimen.

The Ethics Committee at Sohag University approved this study protocol and written consent was taken from all patients.

Kits supplied by Roche (Mannhein, Germany) was used to test serum and ascitic albumin, and seum bilirubin, ALT, AST and alkaline phosphatase spectrophotometrically, and ascetic fluid carcinoembryonic antigen (CEA) was assayed by Simple Step ELISA Kit from Abcam.

Total ADA assay

ADA activity was determined by the described spectrophotometric method.[16] Adenosine was used as a substrate and the amount of ammonia formed was measured by its reaction with phenol nitroprusside and alkaline hypochloride producing blue color that was read spectrophotometrically against water at 628 nm and ADA activity was calculated as U L^{-1} (Berthelot's reaction).[16]

ADA isoenzymes assay

All the three ADA isoenzymes (ADA1c, ADA1m and ADA2) were quantified by using the described polyacrylamide gel electrophoretic technique.[17,18]

For a 5 % gel, a phosphate buffer system consisting of a 0.1M bridge buffer and a 0.05 M gel buffer at pH 6.7 was used. 10 µl of the samples were applied to the gel. Electrophoresis was carried out horizontally at 200 mA for 2.5 hours at 4 °C. To make the isoenzymes visible an ADA staining reaction was used. The staining reaction mixture consisted of the following: 24 mg adenosine (Sigma), 1 U of nucleoside phosphorylase, and 0.5 U of xanthine oxidase (Boehringer), 12 mg 3-(4,5–dimethylthiazol-2-yl)-2,5-diphenyl-2H-tetrazolium bromide salt (Sigma), 1 mg phenazine methosulphate (Sigma) and 16 mg sodium phosphate in 8 ml staining buffer (0.3 M Tris, 0.2 M histidine HCl, pH 7.8). A cellulose acetate sheet soaked with this mixture was applied to the gel and incubated at 37 °C for 60 min.[19] The relative activity of each isoenzyme, determined by densitometric scanning, and the total ADA activity, determined with the spectrophotometric method, were then used to quantify each fraction.

Statistical analysis

Values for variables were presented as mean ± SD with ranges using *t*- test. *P* value less than 0.05 was considered as statistically significant. Data were analyzed using SPSS ver. 10. Sensitivity, specificity and efficiency were statistically calculated.

Results

Ninety two patients with ascites were diagnosed by abdominal ultrasonography and abdominal CT scan was selected. Of that population, 15 patients were diagnosed as parinfection (non TB or malignant ascites), 25 patients were diagnosed as TBP, 21 patients were diagnosed as malignant ascites due to primary or secondary abdominal tumors and the remaining 31 paitents with ascites secondary to liver cirrhosis. Parainfection ascites were secondary to congestive heart failure (5 cases), chronic renal failure (4 cases), continuous ambulatory peritoneal dialysis peritonitis (2 cases), systemic lupus erythematosus (SLE; 2 cases), or chronic pancreatitis (2 cases). Abdominal tumors group included 5 ovarian adenocarcinoma, 4 pancreatic cancers, 3 colorectal cancers, 3 advanced gastric cancers and 6 malignancies of unknown origin.

General clinical and laboratory characteristic of patients are shown in Table 1. Abdominal pain was the main complaint in parainfective ascites but, abdominal distension was apparent in liver cirrhosis, abdominal cancer and TB peritonitis. The complaints started from less than one month before in parainf and abdominal cancer groups than other groups. Laboratory characteristics showed significant low serum albumin and high serum bilirubin, ALT and AST in ascites secondary to liver cirrhosis. Also, SAAG was significantly higher in LC than other groups. Tumor marker (cercinoembryonic antigen; CEA) in ascites was significantly higher in abdominal cancer than other groups.

Table 2 lists the mean standard deviation (SD) and range of total ADA and its isoenzymes (ADA1m, ADA1c and ADA2) in ascitic fluids of patients with parainf, TB peritonitis, abdominal cancer and liver cirrhosis that were electrophoretically separated and photographed (Figure 1). All the tuberculous ascites had total ascitic fluid ADA activities of 41 U L^{-1} or more, whereas one of 21 peritoneal cancer cases and another one in parainf had ADA activities above this level (Figure 2). With diagnostic thresholds of 41 U L^{-1}, the sensitivity, specificity and efficiency of total ADA for tuberculosis were 100 %, 97 and 97.8 %, respectively. Also, ascitic fluid ADA2 activities of 32 U L^{-1} or more were found in 24 TB peritonitis and one abdominal cancer case. With diagnostic thresholds of 32 U L^{-1} of ADA2 in TB peritonitis, the sensitivity, specificity and efficiency of total ADA for tuberculosis were 96 %, 98.5 and 97.8 %, respectively. ADA2/ADA ratio more than 50 % had been found in 22 TB peritonitis and 3 peritoneal cancer case. With diagnostic thresholds of ADA2/ADA ratio more than 50 % in TB peritonitis, the sensitivity, specificity and efficiency of total ADA for tuberculosis were 88 %, 95.5 and 93.4 %, respectively. Less than 5.5 percent difference between the efficiency of ADA, ADA2 and ADA2/ADA ratio was significant.

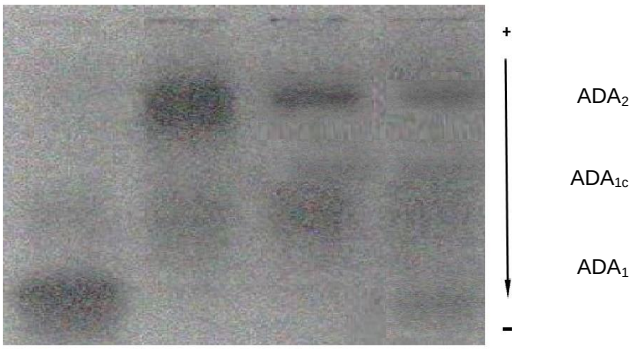

Figure 1. Photography of the electrophoretic pattern of ADA isoenzymes found in ascetic fluids parainfection (parainf), tuberculous peritonitis (TBP), abdominal cancer (AC) and liver cirrhosis (LC).

Table 1. General, clinical and laboratory characteristic patients with ascites with different etiology.

	Parainf *N* (15)	**TBP** *N* (25)	**AC** *N* (21)	**LC** *N* (31)
Age	45.4± 11.5	49.6± 13.6	54.9*± 14.6	38.7± 20.9
Gender (M/F)	(6/9)	(11/14)	(12/9)	(19/12)
Duration of symptoms (%)				
< 1 month	66.7	44	81	32.3
≥ 1 month	33.3	56	19	67.7
Abdominal pain	11 (73.3%)	2 (8 %)	7 (33.3 %)	2 (6.5 %)
Abdominal distension	3 (20 %)	22 (88 %)	19 (90.5 %)	30 (97 %)
Weight loss	1 (6.7 %)	20 (80 %)	18 (85.7 %)	12 (38.7 %)
Fever	9 (60 %)	5 (20 %)	3 (14.3 %)	8 (25.8 %)
Night sweating	1 (6.7 %)	16 (64 %)	1 (4.8 %)	1 (3.2 %)
Loss of appetite	1 (6.7 %)	22 (88 %)	19 (90.5 %)	13 (41.9 %)
Diarrhea	3 (20 %)	13 (52 %)	2 (9.5 %)	1 (3.2 %)
Serum albumin (g L^{-1})	39 ±14	41 ± 12	45± 12	21± 5*
Serum bilirubin				
Total (mg L^{-1})	10 ± 4	9± 3	13± 6	33± 27*
Direct (mg L^{-1})	2± 0.8	3± 0.6	3 ± 1	13± 5 *
Serum ALT (IU L^{-1})	22 ± 13.1	21± 12.3	28± 11.6	51.5± 23.1*
Serum AST (IU L^{-1})	20 ± 11.5	22 ± 14.2	26± 12.6	74 ± 13.1*
Serum alk. Ph. (IU L^{-1})	162± 12.6	156± 17.8	188± 22.3	144± 18.1
Ascitic leukocytes (mm^{-3})	3542.8± 342.2	5739.9± 253.7©	3645.8± 442.9	3101.5± 312.4
Ascitic lymphocytes (%)	23.5± 9.1	69.5± 16.9®	59.4± 15.3	21.4± 5.2
Ascitic albumin (g L^{-1})	28± 23	33± 19	38± 17	4± 2*
SAAG (g L^{-1})	11± 6.2	8.2± 2.4	7.3± 3.7	17.3± 5.3*
Ascitic CEA (ng mL^{-1})	3.4± 2	4.2± 2.1	579.3± 192.7∞	7.3± 4.7

alk. Ph: alkaline phosphatase; ALT: alanine transaminase; AST: aspartate transaminase; CEA: Carcinoembryonic antigen; M/F: Male/female; SAAG: Serum-ascites albumin gradient; *Significant change between LC group and other three groups. © Significant change between TB group and other three groups. ® Significant change between TB group and parainf and LC groups. ∞ Significant change between AC group and other three groups.

Table 2. Adenosine deaminase (ADA) activity in ascetic fluid.

	Total ADA (U L^{-1})		**ADA isoenzymes (U L^{-1})**					
			ADA_{1m}		**ADA_{1c}**		**ADA_2**	
	Mean ±SD	**Range**	**Mean ±SD**	**Range**	**Mean ±SD**	**Range**	**Mean ±SD**	**Range**
Parainf	34.5± 11.1	22-50	24.5± 11.1*	13-40.2	7.8± 3	2.4- 10.5	2.2± 3.9	1- 6.7
TBP	86.7± 23.6	41-130	4.3± 1.9	1.5- 6.3	16.5± 6.2	12.2- 19.4	65.9± 33.5©	31.9-104
AC	32.7± 10.1	22-44	2.8± 2.2	2.9- 7.8	4.7± 1.3	11.3- 26.1	26.2± 6.2®	18.3- 32.7
LC	28.5± 7.3	22-40.5	5.1± 1.3	3.8- 6.9	10.1± 3.3∞	6,2- 12.1	13.3± 9.7¥	10.2- 16.6

*Significant change between ADA_{1m} and other two isoenzymes in parainf. ©Significant change between ADA_2 and other two isoenzymes in TBP. ®Significant change between ADA_2 and other two isoenzymes in AC. ∞Significant change between ADA_{1c} and ADA_{1m} in LC. ¥Significant change between ADA_2 and ADA_{1m} in LC. ADA: Adenosine deaminase;

ADA1m/ADA ratio more than 50 % had been found in 14 parainf cases. With diagnostic thresholds of ADA1m/ADA ratio more than 50 % in parainf cases, the sensitivity, specificity and efficiency were 93.3 %, 100 and 97.8 %, respectively.

Total ascitic ADA < 41 U L^{-1} and ADA2/ADA ratio more than 50 % had been found in 20 cases of AC. With diagnostic thresholds of total ascitic ADA < 41 U L^{-1} and ADA2/ADA ratio more than 50 % in AC cases, the sensitivity, specificity and efficiency were 95.2 %, 100 and 98.9 %, respectively.

ADA deficient patients show defective cell mediated and humoral immunity.[6] The enzyme activity is more potent in T lymphocytes than B lymphocytes and is inversly proportional to the degree of T cell differentiation.[7] High serum ADA activity was reported in patients with some diseases in which cellular immunity is stimulated.[8] The increased serum ADA enzyme activity was detected in tuberculous patients secondary to activation of cell mediated immune system.[20]

Discussion

Lymphocytes and monocytes had comparable levels of ADA activity than other cell types or tissues. All the ADA activity in lymphocytes was attributed to ADA1 (ADA1m and ADA1c). The ADA2 was found only in monocytes.[13] ADA1m contributed approximately to 80 % to the total ADA activity, the residual activity was due to ADA2, with no ADAlc activity present in sputum of tuberculous patients.[14] Therefore, the finding in the current study is that the elevated ADA activity in TB peritonitis may be

secondary to stimulation in cellular immunity.[15] Also, ADA activity in tuberculous ascites was mainly due to ADA2 provides strong evidence that the ADA originates from the monocyte-macrophage cells either due to its turnover or activity.[6]

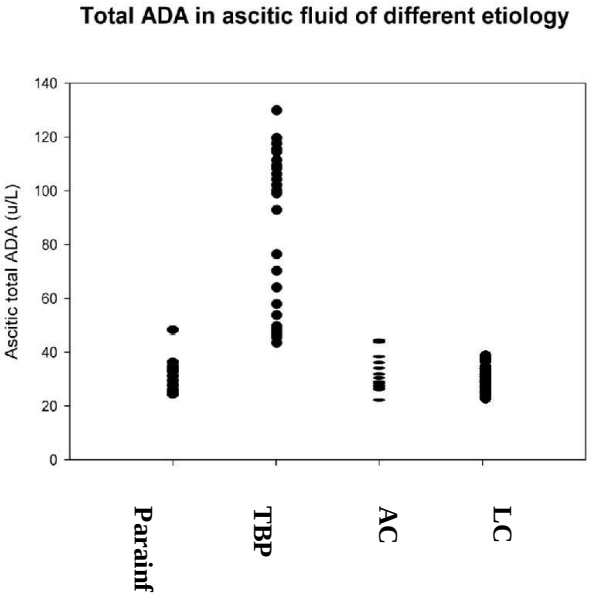

Figure 2. Total ADA activity of ascetic fluids in parainfection (parainf), tuberculous peritonitis (TBP), abdominal cancer (AC) and liver cirrhosis (LC).

The parainfective ascites cases exhibited elevated ADA levels, and the analysis of the isoenzymes profile proved that ADA1m was the predominant form contributing 71 percent of total ADA activity and 76 percent to ADA1 activity. These findings may be attributed to insufficient combining protein needed to convert all ADA1m to ADA1c was present. [5]

The differences in isoenzyme patterns between ascites of different etiologies could be indicative of different origins of ADA, or different mechanisms of release.[14] In the parainfective ascites, ADA probably originates from lymphocytes or neutrophils but, in TB peritonitis, macrophages derived monocytes were the most abundant cell type found in this type of ascites.

The elevated ADA activity in TB peritonitis may be secondary to stimulation in cellular immunity.[12]

The elevated ADA activity in ascites secondary to abdominal tumours may be due to increase in nucleic acid catabolism.[15]

Determination of ADA isoenzymes could help in distinguishing between different causes of ascites, especially between parainfective and non-parainfectve causes as found in this study.

Moreover TB peritonitis could be distinguished from other non-parainfective causes by high total ADA activities of 41 U/L or more (sensitivity, specificity and efficiency were 100 %, 97 and 97.8 %, respectively).

References

[1]Saleh, M. A., Hammad, E., Ramadan, M. M., Abd El-Rahman, A., Enein, A. F. *J. Med. Microbiol*., **2012,** *61(Pt 4)*, 514-9.

[2]Sharma, S. K., Tahir, M., Mohan, A., Smith-Rohrberg, D., Mishra, H. K., Pandey, R. M., *J. Interferon Cytokine Res.*, **2006**, *26(7)*, 484-8.

[3]Ogata, Y., Aoe, K., Hiraki, A., Murakami, K., Kishino, D., Chikamori, K., Maeda, T., Ueoka, H., Kiura, K.,Tanimoto, M., *Acta Med. Okayama.*, **2011**, *65(4)*, 259-63.

[4]Adali, E., Dulger, C., Kolusari, A., Kurdoglu, M. and Yildizhan, R. *Arch. Gynecol. Obstet*., **2009**, *280(5)*, 867-8.

[5]Lee, Y. C., Rogers, J. T., Rodriguez, R. M., Miller, K. D., Light, R. W., *Chest*, **2001**, *120(2)*, 356-61.

[6]Devkota, K. C., Shyam, B. K., Sherpa, K., Ghimire, P., Sherpa, M. T., Shrestha, R., Gautam, S., *Nepal. Med. Coll. J.*, **2012**, *14(2)*, 149-52.

[7]Porcel, J. M., Esquerda, A., Bielsa, S., *Eur. J. Intern. Med.*, **2010**, *21(5)*, 419-23.

[8]Neves, D. D., Dias, R. M., da Cunha, A. J., Preza, P. C., Braz J., *Infect Dis*., **2004,** *8(4)*, 311-8.

[9]Segura, R. M., Pascual, C., Ocaña, I., Martínez-Vázquez, J. M., Ribera, E., Ruiz, I., Pelegrí, M. D., *Clin. Bio-chem*., **1986,** *22*, 141-148.

[10]Pettersson, T., Klockars, M., Weber, T. H., Somer, H., *Scand. J. Infect. Dis*., **1991,** *23*, 97-100

[11]Kosseifi, S., Hoskere, G., Roy, TM., Byrd, RP. Jr., Mehta, J., *South. Med. J*., **2009**, *102*, 57-59.

[12]Dimakou, K., Hillas, G., Bakakos, P., *Int. J. Tuberc. Lung Dis.*, **2009**, *13(6)*, 744-8.

[13]Kayacan, O., Karnak, D., Delibalta, M., Beder, S., Karaca, L., Tutkak, H., *Respir Med*., **2002**, *96(7)*, 536-41.

[14]Dilmaç, A., Uçoluk, GO., Uğurman, F., Gözü, A., Akkalyoncu, B., Eryilmaz, T., Samurkaşoğlu, B., *Respir. Med.*, **2002**, *96(8)*, 632-4.

[15]Lee, S. H., Lee, E. J., Min, K. H., Hur, G. Y., Lee, S. Y., Kim, J. H., Shin, C., Shim, J. J., In, K. H., Kang, K. H., Lee, S. Y., *Clin. Biochem*., **2013**, *46(15)*, 1484-8.

[16]Giusti, G., Galanti, B., *Colorimetric method.* In: Bergmeyer. H. U., ed. *Methods of Enzymatic Analysis*, 3rd edn. Weinheim, *Verlag Chemie*., **1984**, 315-323.

[17]Buel, E. and MacQuarrie, R.. *Prep. Biochem*., **1981**, *11*, 363-80.

[18]Ungerer, J. P., Oosthuizen, H. M., Bissbort, S. H., Vermaak, W. J., *Clin. Chem*., **1992**, *38*, 1322–6.

[19]Spencer, N., Hopkinson, D. A., Harris H., *Ann. Hum. Genet.*, **1968**, *32*, 9-14.

[20]Bhargava, D. K., Gupta, M., Nijhawan, S., Dasarathy, S., Kushwaha, A. K. *Tubercle.*, **1990,** *71(2)*, 121-6.

Received: 16.11.2015.
Accepted: 19.01.2016.

CATALYSIS BY TRIFLIC ACID: SYNTHESIS OF THE INDOLYLQUINONES AS POTENTIAL ANTITUMOR AGENT

Feyriel Dridi[a,b], Didier Villemin [a]*, Nathalie Bar[a], Messaoud Hachemi[b] and Remi Legay[a]

Keywords: *p*-Quinones, indoles, trifluoromethanesulfonic acid, indol-3-ylbenzoquinones.

Trifluoromethanesulfonic acid efficiently catalyzes the conjugate addition of indoles to *p*-benzoquinones under mild conditions affording the corresponding indolylquinones in high yields with high selectivity. In particular, the poorly reactive menadione underwent reaction with indoles under similar conditions to give 3-indolylnaphthoquinones.

* Corresponding Authors
E-Mail: villemin@ensicaen.fr
[a] Laboratoire de Chimie Moléculaire et Thioorganique, UMR CNRS 6507, INC3M, FR 3038, Labex EMC3, Labex Synorg, ENSICAEN & Université de Caen, 14050 Caen, France
[b] Laboratoire de Chimie Moléculaire et Composites, Faculté des Sciences de l'Ingénieur, Université M' Hamed, Boumerdes, Algérie

Introduction

Protonation of quinones with a Bronsted acid (HX) gives a carbocation which can react with different nucleophiles, and after rearomatization the resulting product is a substituted resorcinol. This reaction is well known and already reported for many years with hydrogen halides,[2] hydrogen cyanide,[3] hydrazoic acid,[4] sulphur acids,[5] (thiols, thiourea, sulphite) and amines.[6] The probable mechanism of the reaction of benzoquinone **1** with indole begins by the protonation of benzoquinone, leading to carbon electrophiles (**1β**,**1γ**). Indole reacts with **1γ** as nucleophile and gives indoylhydroquinone in the first step.

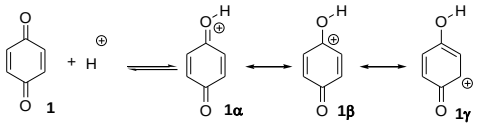

Scheme 1. Protonation of quinones.

After an oxidation step, the resulting indoylquinone can react in a similar way with a second equivalent of indole providing bisindoylhydroquinones. Moreover, in this step, two isomers are likely to be formed. As hydroquinones, bisindoylhydroquinones can be oxidated to bis(indoyl)quinones. As a result, the reaction of indoles with quinones is complex and a mixture of products is generally obtained which need laborious separation.[7]

In fact, the nucleophile addition of indoles on quinones is strongly dependant of the nature of the quinone because the limiting step is the protonation of quinone.

With the easily protonated benzoquinone, the reaction can take place without acid, even in water or with poor acidic agent.[8] With naphthoquinone, a stronger acid is necessary and this reaction was already described with different protic acids,[9] like hydrochloric acid,[9a] tosylic acid.[9c] With methylnaphthoquinone (menadione) the reaction is very difficult. Concerning the reactivity of quinones, the same results were previously observed with the Thiele reaction which can take place from the same carbocation intermediate.[10] This reactivity depends of the basicity of quinone and the electrophilicity of protoned quinone. The reaction with indoles depends also of the nucleophilicity of indoles.[11]

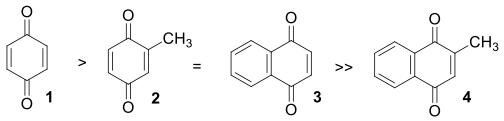

Figure 1. Order of reactivity of quinones.

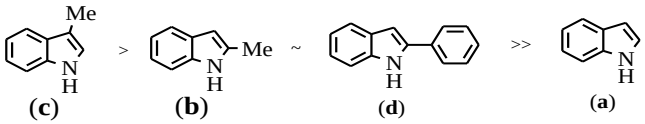

Figure 2. Order of reactivity of indoles.

During our studies on Thiele acetylation of menadione,[11] triflic acid (trifluromethanesulphonic acd, TfOH) was found to be a particularly convenient catalyst, able to broader the synthetic scope of quinones substituted with electron donating groups.

In this context, we decided to investigate the addition of indoles as nucleophile on quinones, in particular methylquinone, naphthoquinone and methyl-naphthoquinone catalyzed by TfOH which has not been reported in the literature.

Experimental

General procedure

A mixture of the quinone (2 mmol) and TfOH (2 mol %) and indole (1 mmol) in dichloromethane (30 mL) was stirred at room temperature under nitrogen for the specified time (Table 1). After completion of the reaction as indicated by TLC, the reaction mixture was quenched with water (15 mL). Sodium carbonate (2 g) was added to the reaction mixture. After filtration, the reaction mixture was extracted with ethyl acetate (2 x 10 mL). The organic phases were combined, dried over Na_2SO_4, and concentrated in vacuum. The resulting product was purified by column chromatography on silica gel (Merck, 100-200 mesh, ethyl acetate-cyclohexane, 0.5-9.5) to afford pure indol-3yl-benzoquinone. Spectral data for selected products are given below.

Table 1. Trifluoromethanesulfonic acid catalyzed reaction of indoles to quinones.

No.	Indole	Quinone	Product	Time, h	Yield[a], %
1	a	3	**3a**	24	47
2	b	3	**3b**	0.25	51
3	c	3	**3c**	0.33	47
4	d	3	**3d**	0.33	48
5	b	2	**2αb, 2βb**	24	36/36
6	c	2	**2αc**	24	45
7	d	2	**2βd**	24	55
8	b	4	**4b 4γ**	24	45/10
9	d	4	**4d**	24	50

[a] Isolated products, except for the mixture 2αb, 2βb determined by NMR (ratio1:1)

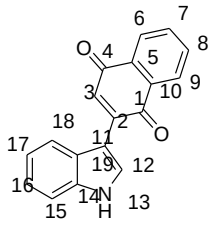

(**3a**)

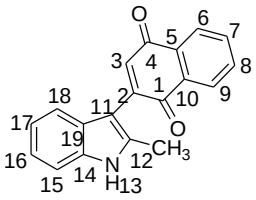

(**3b**)

2-(1*H*-Indol-3-yl)-1,4-naphthoquinone (3a)

M. P. 205-206 °C. IR: 3239, 1589, 1556, 1255, 1230 cm^{-1}. ^1H NMR ($CDCl_3$) : δ = 8.53 (s, 1H, NH_{13}), 8.05 (d, *J=3.2 Hz* 1H, H_{12}), 7.98-7.95 (m, 1H, H_9), 7.94-7.91 (m, 1H, H_6), 7.81-7.76 (m, 1H, H_{18}), 7.58-7.51 (m, 2H, $H_{7,8}$), 7.29-7.23 (m, 1H, H_{17}), 7.46 (s, 1H, H_3), 7.13-7.06 (m, 2H, $H_{16,17}$). ^{13}C NMR ($CDCl_3$) : δ = 185.7 (C1), 185.4 (C4), 142.2 (C11), 136.5 (C14), 133.9 (C7), 133.5 (C8), 133.1 (C10), 132.4 (C5), 131.1 (C12), 129.9 (C3), 127.0 (C9), 125.9 (C6), 125.7 (C19), 123.5 (C16), 122.0 (C17), 120.6 (C18), 112.0 (C15), 109.2 (C2). EIMS: m/z (%): 274 M+H (60), 257 (15), 246 (100), 218 (10). HRMS calcd for $C_{18}H_{12}NO_2$ [M+H]: 274.0868, found: 274.0868.

2-(2-Methyl-3-indolyl)-1,4-naphthoquinone (3b)

M. P. 183-184 °C. IR : 3354, 1617, 1667, 1634, 1565, 1296, 1253 cm^{-1}. ^1H NMR ($CDCl_3$): δ = 8.36 (s, 1H, NH_{13}), 8.22-8.17 (m, 1H, H_9), 8.18-8.13 (m, 1H, H_6), 7.81-7.74 (m, 2H, $H_{7,8}$), 7.54 (d, *J=6.8 Hz*, 1H, H_{18}), 7.34 (d, *J=6.8 Hz*, 1H, H_{15}), 7.22-7.12 (m, 2H, $H_{16,17}$), 7.10 (s, 1H, H_3), 2.48 (s, 3H, CH_3, H_{20}). ^{13}C NMR ($CDCl_3$): δ = 185.3 (C1), 184.6 (C4), 144.4 (C2), 136.9 (C12), 135.5 (C14), 134.8 (C3), 133.7 (C7), 133.5 (C8), 132.8 (C10), 132.3 (C5), 127.7 (C19), 127.0 (C9), 125.9 (C6), 122.3 (C16), 120.9 (C17), 119.3 (C18), 110.6 (C15), 107.4 (C11), 14.0 (C20). EIMS: m/z (%): 288 M+H (25), 270 (100), 260 (15), 242 (25), 117 (10). HRMS calcd for $C_{19}H_{13}NO_2$ [M+1] : 288.1025, found: 288.1018.

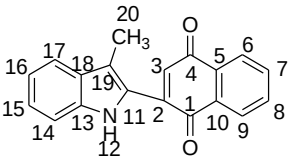

(**3c**)

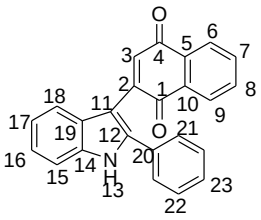

(**3d**)

1-(3-Methyl-2-indolyl)-1,4-naphthoquinone (3c)

M. P. 205-206 °C. IR: 3385, 1644, 1588, 1563, 1331, 1301, 1253 cm^{-1}. ^1H NMR ($CDCl_3$): δ = 10.45 (s, 1H, NH_{12}), 8.19 (d, *J=6.5 Hz*, 1H, H_6), 8.13 (d, *J=6.5 Hz*, 1H, H_9), 7.81-7.79 (m, 2H, $H_{7,8}$), 7.65 (d, *J= 7.8 Hz*, 1H, H_{17}), 7.43 (d, *J= 7.8 Hz*, 1H, H_{14}), 7.29 (t, *J= 7.8 Hz*, 2H, H_{15}), 7.27 (s, 1H, H_3), 7.14 (t, *J= 7.8 Hz*, 1H, H_{16}), 2.62 (s, 3H, CH_3,H_{20}). ^{13}C NMR ($CDCl_3$): δ = 187.7 (C4), 184.6 (C1), 137.4 (C13), 137.3 (C2), 134.5 (C7), 133.7 (C8), 132.5 (C10), 132.1 (C5), 131.6 (C3), 128.6 (C18), 127.1 (C6), 127.0 (C11), 126.0 (C9), 125.3 (C15), 120.16 (C16), 119.9 (C17), 118.7 (C19), 111.8 (C14), 12.6 (C20). EIMS: m/z (%): 288 M+H (80), 270 (100), 260 (20), 242 (15), 235 (5). HRMS calcd for $C_{19}H_{13}NO_2$ [M+1] : 288.1025, found: 288.1018.

2-(2-Phenyl-3-indolyl)-1,4-naphthoquinone (3d)

M. P. 213-214 °C. IR: 3406, 1667, 1647, 1591, 1449, 1294 cm^{-1}. ^1H NMR ($CDCl_3$): δ = 9.30 (s, 1H, NH_{13}), 8.12 (dd, *J=7.6 Hz*, *J=1.2 Hz*, 1H, H_6), 7.95 (dd, *J= 7.6 Hz*, *J=1.2 Hz*, 1H, H_9), 7.75 (td, *J= 7.6 Hz*, *J= 1.2 Hz*, 1H, H_7), 7.69 (td, *J= 7.6 Hz*, *J= 1.2 Hz*, *1H*, *H_8)*, 7.61 (d, *J=7.2 Hz*, 1H, H_{18}), 7.46-7.42 (m, 2H, H_{21}), 7.39 (d, J=7.2 Hz, 1H, H_{15}), 7.33-7.28 (m, 3H, $H_{22,23}$), 7.24 (t, *J= 7.6 Hz*, 1H, H_{16}), 7.22 (d, *J= 7.6 Hz*, 1H, H_{17}), 7.18 (s, 1H, H_3). ^{13}C NMR ($CDCl_3$): δ = 185.2 (C4), 184.2 (C1), 145.2 (C2), 139.5(C12), 136.3 (C14), 135.8 (C3), 133.7 (C7), 133.6 (C8), 132.9 (C10), 132.6 (C20), 132.3 (C5), 128.9 (C22), 128.4 (C23), 128.2 (C19), 128.1 (C21), 126.9 (C9), 125.9 (C6), 123.1 (C16), 121.3 (C17), 119.5 (C18), 111.53 (C15), 106.8 (C11). EIMS: m/z (%): 350 M+H (100), 332 (40), 304 (30), 280 (20), 133 (10). HRMS calcd for $C_{24}H_{16}NO_2$ [M+H] : 350.1181, found: 350.1194.

 DOI: 10.17628/ecb.2015.4.543-547

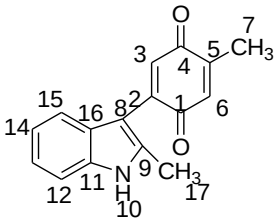

(**2αb**)

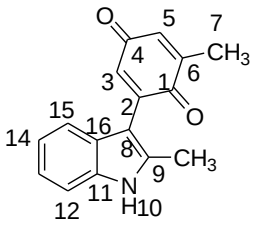

(**2βb**)

2-Methyl-5-(2-methyl-1H-indol-3-yl)cyclohexa-2,5-diene-1,4-dione (2αb)

M. P. 206-208 °C. IR: 3295, 1646, 1603, 1588, 1575, 1457, 1421, 1302, 1244 cm^{-1}. ^1H NMR (DMSO): 11.56 (s, 1H, NH_{10}), 7.36 (d, *J= 7.6 Hz*, 1H, H_{15}), 7.32 (d, *J= 8.0 Hz*, 1H, H_{12}), 7.07 (t, *J= 7.2 Hz*, 1H, H_{13}), 7.00 (t, *J= 8.0 Hz*, 1H, H_{14}), 6.84-6.82 (m, 1H, H_6), 6.74 (s, 1H, H_3), 2.36 (s, 3H, CH_3, H_{17}), 2.03 (d, *J= 1.2 Hz*, 3H, CH_3, H_7). ^{13}C NMR (DMSO): 187.6 (C1), 186.8 (C4), 145.1 (C5), 142.3 (C2), 137.9 (C9), 135.5 (C11), 133.5 (C6), 131.1 (C3), 127.3 (C16), 121.2 (C13), 119.8 (C14), 118.9 (C15), 110.9 (C12), 105.6 (C8), 15.0 (C7), 13.2 (C17). EIMS: m/z (%): 252 M+H (50), 237 (100), 235 (60), 220 (30), 207 (10). HRMS calcd for $C_{16}H_{14}NO_2$ [M+1] : 252.1027, found : 252.1025.

2-Methyl-6-(2-methyl-1H-indol-3-yl)cyclohexa-2,5-diene-1,4-dione (2βb)

M. P. 206-208 °C. IR: 3295, 1646, 1603, 1588, 1575, 1457, 1421, 1302, 1244, 913 cm^{-1}. ^1H NMR (DMSO): 11.56 (s, 1H, NH_{10}), 7.36 (d, *J= 7.6 Hz*, 1H, H_{15}), 7.32 (d, *J= 8.0 Hz*, 1H, H_{12}), 7.07 (t, *J= 7.2 Hz*, 1H, H_{13}), 7.00 (t, *J= 8.0 Hz*, 1H, H_{14}), 6.77-6.75 (m, 1H, H_5), 6.67 (d, *J= 2.4 Hz*, 1H, H_3), 2.36 (s, 3H, CH_3, H_{17}), 2.07 (d, *J= 1,6 Hz*, 3H,CH_3, H_7). ^{13}C NMR (DMSO): 187.7 (C1), 186.8 (C4), 146.01 (C5), 142.03 (C2), 135.5 (C9), 135.4 (C11), 132.6 (C6), 130.9 (C3), 127.3 (C16), 121.1 (C13), 119.7 (C14), 118.9 (C15), 110.9 (C12), 105.9 (C8), 15.9 (C7), 13.2 (C17).

2-Methyl-5-(3-methyl-1H-indol-2-yl)cyclohexa-2,5-diene-1,4-dione (2αc)

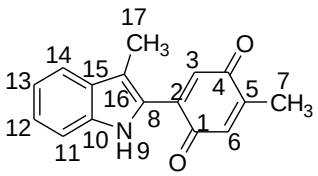

(**2αc**)

M. P. 190-191 °C. IR: 3378, 1617, 1568, 1505, 1330, 1168. ^1H NMR ($CDCl_3$): 10.28 (s, 1H, NH_9), 7.62 (d, *J= 8.0 Hz*, 1H, H_{14}), 7.39 (d, *J= 8.0 Hz*, 1H, H_{11}), 7.27 (t, *J= 8.0 Hz*, 1H, H_{12}), 7.12 (t, *J= 8.0 Hz*, 1H, H_{11}), 7.03 (s, 1H, H_3), 6.67 (q, *J= 1.6 Hz*, 1H, H_6), 2.56 (s, 3H, H_{16}), 2.11 (d, *J= 1.6 Hz*, 3H, H_7). ^{13}C NMR ($CDCl_3$): δ = 190.2 (C1), 187.5 (C4), 146.6 (C5), 137.5 (C10), 135.34 (C2), 133.6 (C6), 128.9 (C3), 128.5 (C15), 126.6 (C8), 125.2 (C12), 120.1 (C13), 119.9 (C14), 118.7 (C16), 111.8 (C11), 15.7 (C7), 12.5 (C17). EIMS: m/z (%): 252 M+H (60), 237 (100), 235 (25). HRMS calcd for $C_{16}H_{14}NO_2$ [M+1] : 252.1025, found: 252.1024.

2-methyl-6-(2-phenyl-1H-indol-3-yl)cyclohexa-2,5-diene-1,4-dione 2βd

^1H NMR ($CDCl_3$): 8.75 (s, 1H, NH_{10}), 7.55 (d, *J= 8.0 Hz* 1H, H_{15}), 7.42-7.31 (m, 6H, $H_{12,18,19,20}$), 7.27 (t, *J= 8.0 Hz*, 1H, H_{13}), 7.22 (t, *J= 8.0 Hz*, 1H, H_{14}), 6.91 (d, *J= 2.6 Hz*, 1H, H_3), 6.64 (dq, *J= 2.6 Hz* , *J= 0.2 Hz*, 1H, H_5); 1.97 (d, *J= 0.2 Hz*, 3H, CH_3, H_7). ^{13}C NMR ($CDCl_3$): 187.8 (C4); 186.8 (C1); 146.5 (C6); 143.2 (C2); 139.1 (C9); 136.3 (C11); 133.6 (C5); 133.4 (C3); 132.7 (C17); 129.1 (C19); 128.6 (C20); 128.2 (C16); 128.1 (C18); 123.3 (C13); 121.5 (C14); 119.6 (C15); 111.5 (C12); 107.0 (C8); 16.5 (C7). EIMS: m/z (%): 314 M+H (60), 299 (100). HRMS calcd for $C_{21}H_{16}NO_2$ [M+1] : 314.1181, found: 314.1177.

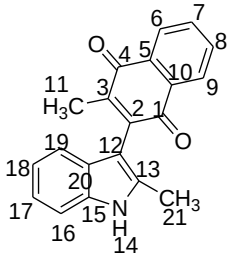

(**4αb**)

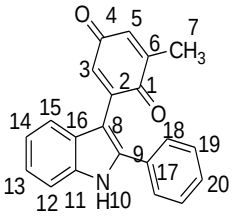

(**2βd**)

2-Methyl-3-(2-methyl-1H-indol-3-yl)naphthalene-1,4-dione (4αb)

M. P. 88-86 °C. IR: 3359, 2923, 1692, 1654, 1593,1458, 1422, 1284 cm^{-1}. ^1H NMR ($CDCl_3$): δ = 8.27 (s, 1H, NH_{14}), 8.20-8.18 (m, 1H, H_6), 8.16-8.14 (m, 1H, H_9), 7.77-7.72 (m, 2H, $H_{7,8}$), 7.31 (d, *J=8.0 Hz*, 1H, H_{16}), 7.18 (d, *J=8.0 Hz*, 1H, H_{19}), 7.15 (t, *J= 8.0 Hz*, 1H, H_{17}), 7.09 (t, *J= 8.0 Hz*, 1H, H_{18}), 2.28 (s, 3H, H_{21}), 2.10 (s, 3H, H_{11}). ^{13}C NMR ($CDCl_3$): δ = 186.0 (C4), 184.0 (C1), 145.8 (C3), 141.07 (C2), 135.6 (C15), 134.8 (C13), 133.6 (C7), 133.5(C8), 132.7 (C10), 132.5 (C5), 128.1 (C20), 126.9 (C9), 126.4 (C6), 121.7 (C17), 120.3 (C18), 119.3 (C19), 110.8 (C16), 106.7 (C18), 15.4 (C12), 13.4 (C21). EIMS: m/z (%): 302 M+H (100), 287 (95), 284 (35), 270 (25), 146 (5). HRMS calcd for $C_{20}H_{16}NO_2$ [M+1] : 302.1181, found: 302.1188.

Results and discussion

The TfOH is a commonly used superacid (*Ho* = -14.1) and is an effective catalyst for many transformations. Its use is preferable to other acids with similar acid strength (e.g. H_2SO_4, $ClSO_3H$, FSO_3H) as it does not promote oxidative side reactions.

In this report, we wish to report a simple, convenient and efficient protocol for the synthesis of indolylnaphtho and benzoquinones using a catalytic amount of TfOH under mild conditions. We have used a ratio quinone/indole = 2:1 in order to favour the formation of monoindoylquinone and to

limit the formation of diindoylindoles. In all cases, the reactions proceeded rapidly in DCM, at room temperature. The products were characterized by ^{1}H, ^{13}C NMR, IR and mass spectroscopic data. We have not studied benzoquinone itself because it reacts rapidly and it is known that benzoquinone is easily protonated by weak acids or even by water.[8,10]

Treatment of 1,4-naphthoquinone **3** with indole in the presence of 2 mol % of TfOH at room temperature gave 2-(3-indolyl)-1,4-naphtoquinone **3a** in 55 % yield. All the reactions of indoles **a-d** with naphthoquinone **3** give pure products, monoindoylnaphthoquinones, with similar yields.

Methylbenzoquinone **2** can lead to the formation of different regioisomers **2α** and **2β**. However in the literature, only the regioisomer **2α** corresponding to a 1,4 attack relative to the methyl has been reported with indole and 2-methylindole. According to the nature of indoles, different results are obtained with triflic acid. For the 3-methylindole, the condensation takes place on the opposite side of the methyl probably due to steric hindrance, and conducts to the expected regioisomer **2αc**. Concerning 2-phenylindole, only the stereoisomer **2β** is produced. On the other hand, 2-methylindole affords the two regioisomers, in equal amount with a total yield of 72 %. In fact, it is not surprising to obtain the regioisomer **2β**, the carbocation corresponding to its formation is the most stabilized by the presence of the methyl group.

In a similar way, 2-methyl-1,4-naphthoquinone (**4**, menadione) afforded 2-(3-indolyl)-1,4-naphthoquinones derivatives **4b** and **4d.** Menadione is less reactive in Thiele-Winter reaction in which the intermediate is the same as in reaction of quinone with indole.

Surprisingly, different results were obtained from the reaction of menadione **4** with 2-methylindole **b**. The naphthoquinone **4** afforded the expected 3-indolylquinone **4b (**2-methyl-3-(2-methyl-1H-indol-3-yl) naphthalene-1,4-dione (45% of yield), along with a small amount (10%) of 2-methyl-4-(2-methyl-1H-indol-3-yl) naphthalen-1-ol **4γ.**

This product **4γ** was already reported in literature and a mechanism of formation has been proposed.[12] The condensation takes place on the carbonyl group of the quinone, followed by an elimination of a molecule of water. A similar reactivity, rather rare, have been observed with hydroxyquinones but not with menadione.

The monoindolyl products, prepared from different indoles and quinones exhibit sometimes pharmaceutical properties as antitumoral properties. Yet, relatively little attention has been focused on this type of compounds contrary to natural diindoylquinones[13] which are well known for their antitumoral properties. Preliminary results show that all products (**3a-3d**) were found active against four types of cancer cell types but **3c** was found particularly active (0.1 μMol) against B16F10.[14]

Conclusion

In conclusion, triflic acid is an excellent catalyst for the synthesis of indolylquinones. Triflic acid exhibits an unusual reactivity with methylquinone and menadione leading to new derivatives which are fully characterized. The monoindolylnaphthoquinones were tested on four types of cancer cells, all of them displayed interesting antiproliferative activity, and the compound **3d** was found as very promising.

Acknowledgments

We gratefully acknowledge the CNRS (National Center for Scientific Research), the "Region Basse Normandie", the University of Boumerdes (Algeria), the Franco-Algerian program for the Superior Education (PROFS), and the Algerian-French cooperation for a BAF grant for Feyriel Dridi. Also the authors thank Baptiste Rigaud for NMR spectra and Mrs. Karine Jarsalé for ESIMS and HRMS analysis. The authors thanks Pr. Marc Lecouvey and Odile Sainte-Catherine (CSPBAT, Bobigny, France) for the preliminary screening on human cell line

References

[1]Finley, K.T. "*The addition and substitution chemistry of quinone*", in *The chemistry of quinonoid compounds*, chap.17, pages 878-1126, S. Patai editor, J. Wiley and Sons, **1974**.

[2]Hinsberg O., Himmelschcin A., *Ber.*, **1896,** *29*, 2023-2029.

[3]Thiele J., Meisenheimer J., *Ber.*, **1900**, *33*, 675-676.

[4]Oliveri-Mandala, E., Calderaro E., *Gaz. Chim. Itat.*, **1915**, *45*, 120, 307.

[5]Hinsberg O., *Ber.*, **1894**, *27*, 3259-3261 ; Hinsberg O., *Ber..*, **1895**, *28*, 1315-1320 ; Snell, J. M., Weissberger, A., *J. Am. Chem. Soc.* **1939**, *6*, 450-453 ; Porter, R. F., Rees, W. W., Frauenglass, H., Wilgus, S., *J. Org. Chem*. **1964**, *29*, 588 - 594.

[6]Suida, H., Suida, W., *Ann. Chem.*, **1918**, *416*, 113-163 .

[7]We are unable to reproduce the selectivities and the yields claimed by Yadav *et al*: Reddy A.V., Ravinder K., Venkateshwar Goud T., Krishnaiah P., Raju T.V., Venkateswarlu Y., *Tetrahedron Letters*; **2003**, *44*, 6257-6260; Yadav J.S., Reddy B.V.S, Swamy.T., *Synthesis*. **2004**, *1*, 106-110.

[8]Hai-Bo Zhang, Li Liu, Yong-Jun Chen, Dong Wang ,Chao-Jun Li, *Eur. J. Org. Chem*., **2006**, *4*, 69-873**.**

[9](a) Mohlau R., Redlich R. *Ber*. **1911**, *44*, 3605-3608; (b) Bu'Lock J. D., Harley-Mason J., *J. Chem. Soc*. **1951**, 703-711; (c) Bruce J. M, *J. Chem. Soc*, **1959**, 2366-2375 ; (c) Maiti A. K., Bhattacharya P., *J. Chem. Res*. (*S*) **1997**, 424-425 (d) Henrion J.C, Jacquet B., Hocquaux M., Lion C., *Bull. Soc. Chem. Belges.*, **1994**, *103*, 163-168

[10](a) Villemin, D.; Hammadi, M.; Bar, N. *Tetrahedron Lett.*, **1997**, *38*, 4777-4778; (b) Villemin, D.; Bar, N.; Hammadi, M; Hachemi, M. *J. Chem. Res. (S),* **2000**, 356-358.

[11]The classification of the nucleophilicities of indols presented here was based on the level of the LUMO of indols obtained by semiempirical MP6 computation: 3-methylindole: -8.16 eV; 2-phenylindole: -8.27 eV; 2-methylindole -8.29 eV; Indole: -8.41 eV. For experimental studies of nucleophilities of indols see: Lakhdar S., Westermaier M., Terrier F. , Goumont R. , Boubaker T. , Ofial A. R. , Mayr H., *J. Org. Chem*., **2006**, *71* , 9088-9095.

[12]Kouloouri S., Malamidou-Xenikaki E., Spyroudis S., *Tetrahedron Lett*., **2005**,10894-10902.

[13](a**)** Shimizu S., Yamamoto Y., Inagaki J., Koshimura S., *Gan.* **1982**, *73*, 642-8; (b) Pirrung M. C., Park K., Li Z., *Org*. *Lett*. **2001**, *3*, 365-367; Pirrung M. C., Deng L., Li Z., Park K. *J*. ,*Org*. *Chem*. **2002**, *67*, 8374-8388; c) Koulouri S., Malamidou-Xenikaki E., Spyroudis S., *Tetrahedron.* **2005**, *61*, 10894-10902.

[14](a) Dridi F., Bar N., Sainte-Catherine O., Hachemi M., Lecouvey M. , Villemin D., *Eur. Chem. Bull.*, **2014,** *3*, 1020-1026, (b) F. Dridi, Ph. D., University of Boumerdès, 2015.

Received: 12.11.2015.
Accepted: 04.02.2016.

AUTOIMMUNE THYROIDITIS IN TYPE 1 DIABETES MELLITUS

Ali Ismaeil Ali Abd Alrheam [a]*, Zafer Saad Al Shehri[a], Heba F. Gomaa[b] and Nasser Badi K Al Mutairi[a]

Keywords: Diabetes mellitus; serum TSH; serum FT3; serum FT4; anti TPO antibodies; anti TG antibodies.

We have compared the frequency of thyroid antibodies among diabetic (DM) patients with type 1 and type 2. Diagnosed type-1 DM patients, having no previous of history were taken as subjects and divided into early adulthood (18 to 35 yrs) and later adulthood (after 35 yrs) groups. Matched subjects with DM type II are taken as controls. In all subjects, serum concentration of free T3 and free T4, TSH, Thyroid peroxidase antibody (TPO-Ab) and Thyroglobulin antibodies (TG-Ab) were determined. It has been observed that the serum FT3 levels was lower in type-1 diabetics patients as compared to type II DM. In addition there was a slightly increase in the values of anti-TPO and anti-TG antibodies in later adult hood of type I DM when compared to the values of early adult hood of type I DM. And there was significant increase in the values of anti-TPO and anti-TG antibodies in later adulthood of type I DM when compare to the values of later adulthood of type II DM. It has been suggested that estimation of thyroid antibodies should be done periodically for every diabetic patients.

* Corresponding Authors
Phone: +966-(0583669016)
E-Mail: a.ismail@su.edu.sa
[a] Clinical Laboratory Science Department College of Applied Medical Sciences (Dawadmi), Shaqra University, Saudi Arabia
[b] Zoology Department, Faculty of science, Ain Shams University, Egypt

Introduction

Diabetes mellitus is a group of metabolic diseases characterized by high blood sugar (glucose) levels that result from defects in insulin secretion, or action, or both. Elevated levels of blood glucose (hyperglycemia) lead to spillage of glucose into the urine, hence the term sweet urine. In 2014 the global prevalence of diabetes was estimated to be 9 % among adults aged (18+ years).[1]

Autoimmune thyroiditis is a group of inflammatory thyroid disorders with either hypothyroid, euthyroid or hyperthyroid state.[2] Diabetes mellitus type 1 is often accompanied by autoimmune diseases. Autoimmune thyroid diseases are amongst the most common.[3,4] Recent studies confirmed an increased incidence of autoimmune thyroid diseases even in type-2 diabetes mellitus. Various experimental, clinical studies as well as genetic and epidemiological studies showed the immunological and genetic basis of relationship between diabetes mellitus and thyroid diseases. Currently there is a lot of evidence about the importance of genetic factors in autoimmune diseases.[5]

At least two major clinical forms of chronic autoimmune thyroiditis can be distinguished, Hashimoto and atrophic. The Hashimoto type is characterized with small goiter, elevated anti-thyroperoxidase antibodies (anti-TPO), less commonly anti-thyroglobulin antibodies (anti-TG), and a typical ultrasound picture of thyroiditis. The function of the thyroid gland can be normal, however hypothyroidism can develop later. The atrophic form is a less common type of chronic autoimmune thyroiditis characterized by early development of hypothyroidism and ultrasound signs of thyroid gland atrophy and production of fibrotic tissue. Serum levels of anti-TPO and anti-TG are also typically elevated.[4]

The coexistence of hypothyroidism might cause disturbances in the metabolic control of patients with diabetes.[6] Even subclinical hypothyroidism (slightly elevated TSH without impairment of T4 and T3 levels) is associated with higher frequency of symptomatic hypoglycemia.[7] This finding can be explained by basis of the well known physiological effects of thyroid metabolism on carbohydrates metabolism. Thyroid hormones stimulate intestinal absorption of glucose, further glycogenolysis and hepatic insulin catabolism are also enhanced. These mechanisms have a hyperglycemic effect and subtle changes in thyroid hormone levels might interfere with these actions, thereby increasing the risk of hypoglycemia.[8,9]

The relationship between type I diabetes mellitus and autoimmune thyroid disease was first described in the early 1960s by Pettit and Landing.[9,10] The association of type 1 diabetes mellitus with autoimmune thyroid disease has been well documented in many populations.[11-15] The occurrence of thyroid autoantibodies against microsomes (AMA) and thyroglobulin (ATA), frequently seen in Hashimoto's thyroiditis and Graves' disease, has also been reported in type 1 diabetes mellitus with varying frequency.[16-18] Several subsequent cross sectional studies from various parts of the world have been reported.[19,20] Type 1 diabetes mellitus may be associated with additional autoimmune disorders including autoimmune thyroid disease,[21] coeliac disease[22] and Addison's disease.[23]

In this study we aimed to compare the frequency of thyroid antibodies among diabetic patients with type 1 and type 2 diabetes.

Materials and methods

Subjects

The samples were collected from the Central hospital, Al-dawadmi, KSA, and measurements were conducted in the Department of Clinical Biochemistry, College of Applied Medical Science, Al-dawadmi, Shaqra university, KSA. Fifty diagnosed type-1 diabetes mellitus patients are chosen for our study. Patients classified into two groups each consists of 25 subjects (M=12, F=13) of early adulthood (18 to 35 yrs) and 25 subjects (M=13, F=12) of later adulthood (after 35 yrs). Twenty-five age matched subjects (M=11, F=14) with diabetes mellitus type II were taken as controls. All the subjects had no history of previous thyroid diseases. Informed consent was obtained from all the subjects. Fasting blood samples were collected by venipuncture technique and for separation of serum, the blood is centrifuged at 3000 rpm for 5 min.

The separated serum is used to estimate serum TSH, FT3, FT4, anti TPO antibodies and anti TG antibodies.

Measurements of anti-TPO (IgG)

Anti-TPO (IgG) was measured by using enzyme linked immunosorbent Sandwich assay (ELISA). The ELISA procedure was done according to the manufacturer's instruction (DRG, Germany). Highly purified human thyroid peroxidase (TPO) was bound to microwells. 100 µl of calibrators, controls and patients sera were added in duplicate to each well and incubated for 30 minutes at room temperature. After washing three times, 100 µl of conjugate (anti-human IgG labeled with horseradish peroxidase) was added to each well and incubated for 15 minutes at room temperature. After washing three times, 100 µl of substrate solution, (Tetramethylbenzidine 'TMB') was added to each well. The reaction mixture was then incubated for 15 minutes at room temperature in the dark. 100 µl of stop solution (1 M hydrochloric acid) was then added to each well. Finally, the optical density was measured using microplate reader instrument (Expert Plus, EC) at 450 nm. The mean absorbance (O. D) for each set of duplicate calibrators, controls and patients sera was calculated. The IgG concentration of the unknown was determined from the standard curve. Any concentration >30 IU mL^{-1} was considered as positive.

Measurements of anti-thyroglobulin (anti-TG-Ab) measurement

Anti-thyroglobulin was measured by using ELISA assay. The ELISA procedure was done according to the manufacturer's instruction (DRG, Germany).

The microwells were coated with purified native human thyroglobulin (hTg). Anti-Tg autoantibodies (TG-Ab), when present in the sample, will bind to the solid phase. After removing non specific antibodies by a washing process, the immune complexes are detected by alkaline phosphatase conjugated polyclonal antibodies to human IgG. After removing the unbound conjugate by another washing step, the chromogen/substrate is added, which turns from clear to yellow color if the antibody being tested is present. The intensity of the yellow color, directly proportional to the amount of antibody present in the patient sample, is measured using a spectrophotometer with a 405 nm filter. Patient sample concentrations are read from a calibration curve.

The mean absorbance (O.D) for each set of duplicate calibrators, controls and patients sera was calculated. The IgG concentration of the unknown was determined from the standard curve. In healthy normal subjects 99 % of all values were below 20 IU mL^{-1}.

Measurement of thyroid stimulating hormone (TSH), free T3 and free T4

Thyroid stimulating hormone (TSH), free T3 (FT3) and free T4 (FT4) were measured by an automated analyzer (Elecsys 2010 platform, Roche Diagnostics GmbH), as per the procedure indicated by the manufacturer.

Statistical Analysis

Comparison between means was performed by Student's *t*-test and comparison between frequencies was carried out by chi-squared test. A '*p*' value of 0.05 or less was interpreted as significant for the analysis.

Results

Data in Table 1 showed that, there was a significant decrease in the values of FT3 in both groups of type I DM when compared to the FT3 values of later adult hood of type II DM (Figure 1). There is no statistical difference in the values of FT4 and TSH between both the groups of type I diabetes mellitus and type II diabetes (Figures 2 and 3).

There was a slight increase in the values of anti-TPO and anti-TG antibodies in later adult hood of type I DM when compared to the values of early adult hood of type I DM. And there was significant increase in the values of anti-TPO and anti-TG antibodies in later adulthood of type I DM. when compare to the values of later adulthood of type II DM (Figures 4 and 5).

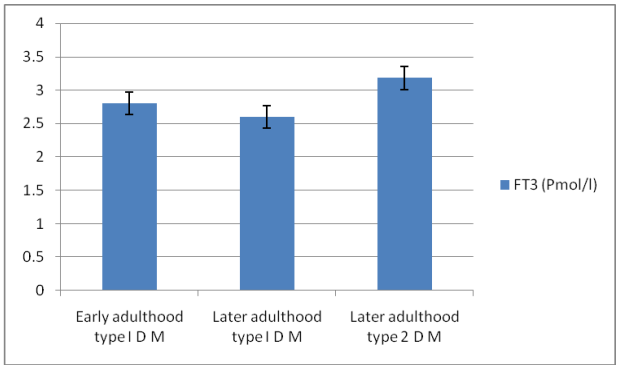

Figure 1. The mean level of free T3 (p mol/l) in different groups.

Table 1. Comparison between mean levels of FT3, FT4, TSH, TP-Ab and TG-Ab.

Parame-ter	Early adulthood DM 1	Later adulthood DM 1	Later adulthood DM 2	'*p*' value
FT3 (pmol L^{-1})	2.8 ± 0.71	2.6 ± 0.67	3.18 ± 1.02	<0.05 S
FT4 (pmol L^{-1})	9.75 ± 0.15	9.81 ± 0.25	9.50 ± 0.05	N.S
TSH (µl U mL^{-1}	3.91 ± 0.25	3.85 ± 0.45	4.1 ± 0.33	N.S
TPO (units)	26.98 ± 2.61	29.28 ± 2.40	19.49 ± 1.92	<0.0001 H.S
TG Ab (units)	25.55 ± 2.20	27.52 ± 1.8	22.75 ± 1.91	<0.0001 H.S

S= Significant, H.S = highly significant, N.S = not significant

From Table 2 we can note that in early adulthood type 1 DM a total 5/25 (20 %) patients had positive TPO antibodies (2 men and 3 women) while only 3/25 (12 %) patients had positive TG antibodies (1 men and 2 women), if we look to late adulthood type 1 DM there are total 7/25 (28 %) patients had positive TPO antibodies (3 men and 4 women) and total 4/25 (16 %) patients (1 men and 3 women) had positive TG antibodies, similarly late adulthood type 2 DM had total of 6/25 (24 %) patients with positive TPO antibodies (3 men and 3 women) and 5/25 (20 %) (2 men and 3 women) patients had positive TG antibodies (Figure 6**)**.

The results (Table 2) also indicate that in the early adulthood type 1 DM the percentage of positive subjects to TPo-Ab is more higher in females 3/13 (23 %) than in males 2/12 (16.6 %). In the late adulthood type 1 DM, the percentage of females positive TPo-Ab is higher 4/12 (33.3 %) than in males 3/13 (23 %) and it is also still higher in late adulthood type 2 DM in female 3/14 (21.4 %) than in males 3/11 (23 %) (Figure 7**)**. We also found (Table 2) that in the early adulthood type 1 DM the percentage of positive subjects to TG-Ab is more higher in females 2/13 (15.3 %) than in males 1/12 (8.3 %).

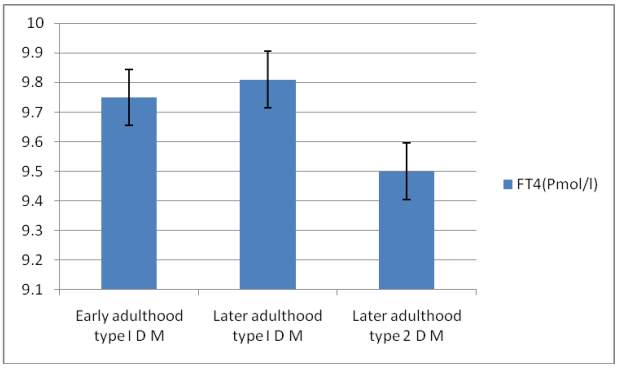

Figure 2. The mean level of free T4 (*p* mol L^{-1}) in different groups.

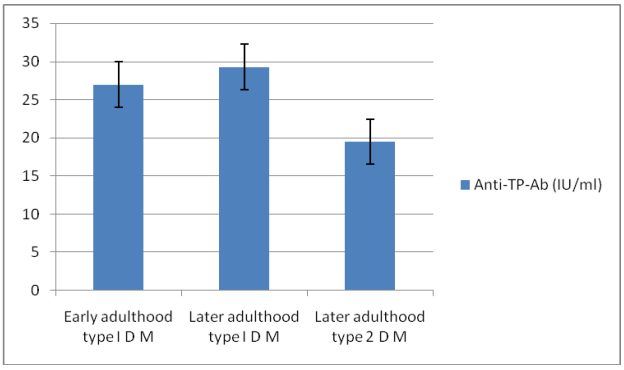

Figure 4. The mean level of TP-Ab (IU mL^{-1}) in different groups.

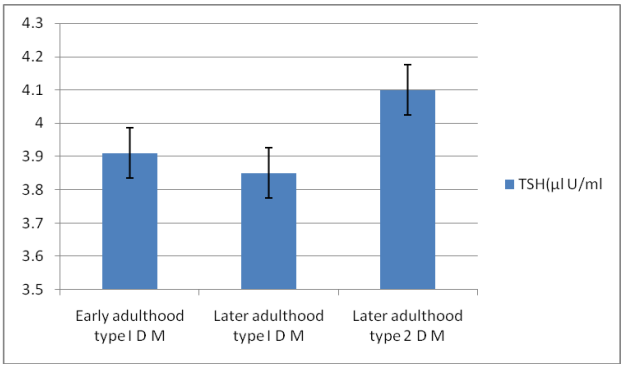

Figure 3. The mean level of TSH (µl U mL^{-1}) in different groups.

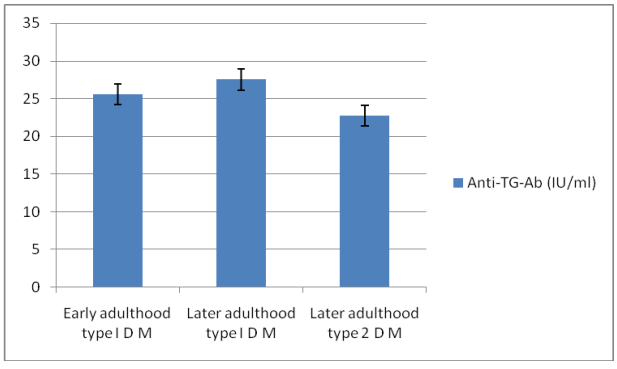

Figure 5. The mean level of TG-Ab (IU mL^{-1}) in different groups

Table 2. Percentage of positive subjects to TPo-Ab and TG-Ab in different diabetic groups.

Group	Item	Male Positive subjects	female Positive subjects	Total
Early adulthood type 1 DM	TPO-Ab	2/12 (20 %)	3/13 (23 %)	5/25 (20 %)
	TG-Ab	1/12 (8.3 %)	2/13 (15.3 %)	3/25 (12 %)
Late adulthood type 1 DM	TPO-Ab	3/13 (23 %)	4/12 (33.3 %)	7/25 (28 %)
	TG-Ab	1/13 (7.6 %)	3/12 (25 %)	4/25 (16 %)
Late adulthood type 2 DM	TPO-Ab	3/11 (23 %)	3/14 (21.4 %)	6/25 (24 %)
	TG-Ab	2/11 (18 %)	3/14 (21.4 %)	5/25 20 %)

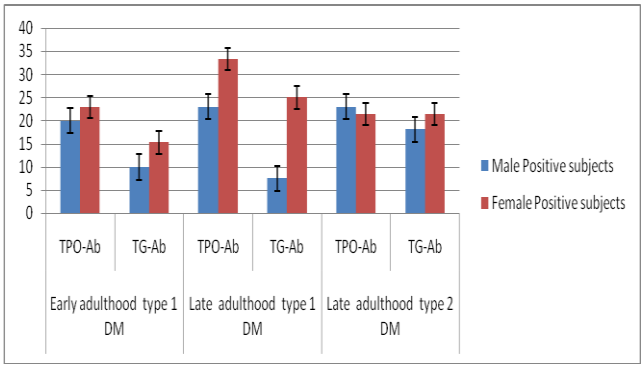

No. of subjects = 25 in each group, Positive TPo-Ab subjects ≥30 IU mL^{-1}

Figure 6. Percentage of male and female subjects positive to TPo-Ab and TG-Ab in early and late adulthood type (1) DM with respect to late adulthood type (2) DM.

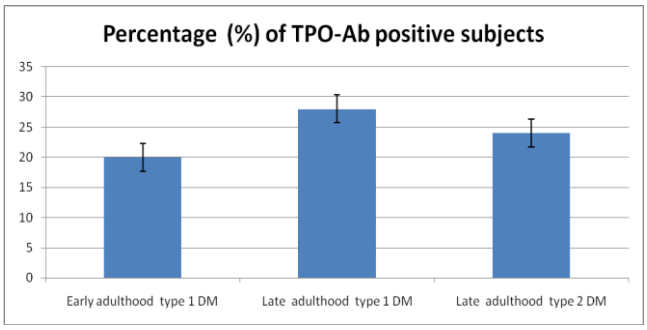

Figure 7. Percentage of TPo-Ab positive subjects in different types of diabetic (No. of subjects = 25 in each group).

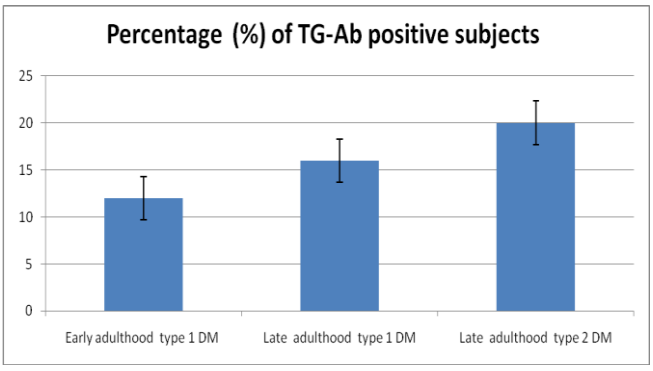

Figure 8. Percentage of TG-Ab positive subjects in different types of diabetic (No. of subjects = 25 in each group).

In the late adulthood type 1 DM, the number of females positive TG-Ab is higher 3/12 (25 %) than in males 1/13 (7.6 %) and it is also still higher in late adulthood type 2 DM in female 3/14 (21.4 %) than in males 2/11 (18.1 %) (Figure 8).

Discussion

Autoimmune diseases combined by development of specific immune response against one or more organs. Many factors are involved including genetic and environmental factors leading to a clinically evident disease.

It is well known that Type 1 diabetes mellitus is an autoimmune disease and can be associated with other autoimmune diseases.[24] Previous studies showed that patients with type 1 diabetes mellitus, is frequently reported to have autoimmune thyroid disease.[25]

In the present study, the serum levels of FT4 and TSH in early and late adulthood type 1 Diabetes Mellitus were not statistically different than that of later adulthood Type II diabetic patients, but the serum FT3 levels were found to be lower in type-1 diabetics as compared to type II diabetes mellitus. The decreased serum level of FT3 may be due to impairment of 5-monodeiodinase enzyme activity, which controls the peripheral conversion of T4 into T3.[26] Guillermo et al found subclinical hypothyroidism in 6.5 % of type-1 diabetic male patients. The likely explanation for this association with thyroid abnormalities is a common underlying predisposition leading to co-existing autoimmune destruction of pancreatic islet cells and autoimmune attack on thyrocytes.[27]

In addition the results showed that, there was a slightly increase in the values of anti-TPO and anti-TG antibodies in later adult hood of type I DM when compared to the values of early adult hood of type I DM. There was significant increase in the values of anti-TPO and anti-TG antibodies in later adulthood of type I DM when compare to the values of later adulthood of type II DM. In agreement with our results, a previous study conducted to determine the level of thyroid autoimmunity among clinically thyroid patients of type 1 and type 2 diabetics and to correlate the levels with pattern of diabetes showed that thyroid autoimmune process seems to be correlated more with type 1 diabetic.[28]

The prevalence of thyroid diseases in diabetic patients was found to be 2-3 times higher than in non-diabetic subjects.[29]

We also observed that in the early adulthood type 1 DM the percentage of positive subjects to TP-Ab and TG-Ab are more higher in females than in males and this with agreement with the previous studies that indicated that organ-specific endocrine autoimmunity develops more frequently in females, including type 1 DM and type 2 DM with thyroid auto-immunity and this may be due to inheritance of the production of serum anti-TPO in an autosomal fashion in females but not in males.[30,31]

The involvement of organ specific antibodies in the pathogenesis of the disease is secondary to tissue destruction by thyroid infiltrating T-cells is still unknown. It is also unclear that whether anti-TPO antibodies are able to induce hypothyroidism by blocking the enzyme thyroid peroxidise.[32]

The benefits of identifying thyroid dysfunction at an early stages as a clinical disorder even in asymptomatic patients are considerable particularly in view of high likely hood of progression to overt thyroid dysfunction. It could be concluded that estimation of thyroid antibodies should be done periodically for every type-1 diabetic patients.[33]

Conclusion

Patients with positive antibodies should be monitored for TSH elevation at yearly intervals with the goal of early detection to prevent the possible adverse effects on the human body metabolism. Without these regular and specific laboratory tests, early diagnosis of autoimmune thyroid diseases in routine diabetologic practice is a very difficult task.

Conflict of interests

All authors have declared that there is no conflict persists in this article.

Acknowledgements

The authors are thankful to Shaqra University, Ministry of Higher Education, Kingdom of Saudi Arabia for funding this research and providing platform to encourage research and developments amongst the students, staff and society. We are also very much thankful to the Department of Clinical Laboratory Science, College of Applied Medical Science Dawadmi, Shaqra University Kingdom of Saudi Arabia for their help with lab facility. We could not have proceeded to this present work if they do not allow us. We again thank their ethical committee for approving our in vivo protocol.

Competing interests

The authors declare that they have no competing interests.

References

[1]WHO, *Global Status Report on Noncommunicable Diseases*, **2014**, World Health Organization, Geneva.

[2]Slatosly J., Shipton, B., Walba, H., *Ann. Fam. Physician*., **2004**, *61*, 1042-1052.

[3]Kinova, S., Paya, J., Kalafutova, I., Kucerova, E. (1998) *Bratisl. Med. J*., **1998**, *99*, 23-25.

[4]Vondra, K., Zamrazil, V., DMEV, **2002**, *5*, 78-84.

[5]Kedari, G. S. R., *Indian J. Sci. Tech*., **2010**, *3*, 1014-1015.

[6]Swift, P. G. F., Ed., *Hypothyroidism*: *Consensus Guidelines*, International Society for Pediatric and Adolescent Diabetes, Medical Forum International, Zeist, **2000**, p. 103.

[7]Mohn, A., Di Michele, S., Di Luzio, R., Tumini, S., Chiarleli, F., *Diabet. Med*., **2002**, *19*, 70-73.

[8]Berant, M., Diamond, E., Mabriki, W., Ben-Yitzhak, O., (1993). *Pediatr. Res*., **1993**, *34*, 79-83.

[9]Prager, C., Cross, H. S., Peterlik, M., (1990). *Acta Endocrinol*., **1990**, *122*, 585-591.

[10]Pettit, M. D., Landing, B. H., Guest, G. M., *J. Clin. Endocrinol. Metab*., **1961**, *21*, 209-10.

[11]Bottazzo, G. F., Mann, J. I., Thorogood, M., Baum, J. D., Doniach, D. (1978) *Brit. Med. J*., **1978**, *2*, 165-168; Landing, B. H., Pettit, M. D., Wiens, R. L., Knoles, H., Guest, G. M., *J. Clin. Endocrinol. Metab*., **1963**, *23*, 119-20.

[12]Riley, W. J., Winer, A., Goldstein, D., *Diabetologia*, **1983**, *24*, 418-421.

[13]Betterle, C., Zanette, F., Pedini, B., Presotto, F., Rapp, L. B., Monciotti, C. M., Rigon, F., *Diabetologia*, **1984**, *26*, 431-436.

[14]Chikuba, N., Akazawa, S., Yamaguchi, Y., Kawasaki, E., Takino, H., Takao, Y., Maeda, Y., Okuno, S., Yamamoto, H., Yokota, A., *Intern. Med*., **1992**, *31*, 1076-1080.

[15]Tsai, W. Y., Lee, J. S., *Diabetes Care*, **1993**, *16*, 1314-1315.

[16]Riley, W., MacLaren, N., Zlezotte, D., Spillar, R., Rosenbloom, A., *J. Pediatr*., **1981**, *98*, 350-354.

[17]Prina, C. L. M., Weber, G., Meschi, F., Mora, S., Bognetti, E., Siragusa, V., Natale, B., *Diabetes Care*, **1994**, *17*, 782-783.

[18]Chuang, L. M., Wu, H. P., Chang, C. C., Tsai, W. Y., Chang, H. M., Tai, T. Y., Lin, B. J., *Clin. Endocrinol*., **1996**, *45*, 631-636.

[19]Kehr, S., Gastauer, R., Wikler, G., (1985). *Mschr. Kinderh*., **1985**, *133*, 738-742.

[20]Frasier, S. D., Penny, R., Snyder, R., Goldstein, I., Graves, D., *Am. J. Dis. Child.* **1986**, *140*, 1278-80.

[21]Perros, P., Crimmon, R. S., Shaw, G., Frier, B. M., *Diabetes Med*., **1995**, *12*, 622-627.

[22]Barera, G., Bonfanti, R., Viscardi, M., *Pediatrics*, **2002**, *109*, 833-838.

[23]Barker, J. M., Ide, A., Hostetler, C., *J. Clin. Endocrinol. Metab*., **2005**, *90*, 128-134.

[24]Redondo, M. J., Eisenbarth, G. S., *Diabetologia*, **2002**, *45*, 605-622.

[25]Ergur, A. T., Oçal, G., Berberoğlu, M., Adıyaman, P., Sıklar, Z., Aycan, Z., Evliyaoğlu, O., Kansu, A., Girgin, N., Ensari, A., *J. Clin. Res. Pediatr. Endocrinol*., **2010**, *2*, 151-154.

[26]Suzuki, Y., Nanno, M., Gemma, R., *Endocrinal. J. Pn*., **1992**, *39*, 445-453.

[27]Umpierrez, G. E., Latif, K. A., Murphy, M. B., Lambeth, H. C., Stentz, F., Bush, A., Kitabchi, A. E., *Diabetes Care*, **2003**, *26*, 1181-1185.

[28]Yasmin, T., Ghafoor, F., Malik, T., Khan, A. U., *J. Coll. Physicians. Surg. Pak*., **2006,** 16, 751-754.

[29]Vondra, K., Vrbikova, J., Dvorakova, K., *Minerva Endocrinol*., **2005**, *30*, 217-236.

[30]Abdullah, H., Bahakim, M.O., Gad Al Rab, K. Halim, H., Salman, A. A., *Diabet. Med*., **1990**, *7*, 50-52.

[31]Philips, D., Prentice, L., Upadhyaya, M., (1991). *J. Clin. Endocrinol. Metab*., **1991**, *72*, 973-975.

[32]Mohn, A., Di Michele, S., Faricelli, R., Martinotti, S., Chiarelli, F., *Eur. J. Endocrinol*., **2005**, *153*, 717-718.

[33]Omara, M. A., Rizkb, M. M., El-Kafourya, A. A., *Alexandria J. Med*., **2014**, *50*, 77-82.

Received: 16.12.2015.
Accepted: 04.02.2016.

A CONVENIENT APPROACH FOR REDUCTION OF SOME FLUORO IMINES USING $NaBH_4$

Avinash T. Shinde,[a]* Sainath .B. Zangade[b] and Yeshwant .B. Vibhute[c]

Keywords: $NaBH_4$ reduction; fluoroamines; fluoroimines; spectral data.

Fluoroimines have been reduced to their corresponding amines by means of $NaBH_4$ using MeOH as a solvent at room temperature. The reaction time and yield are 1-1.5 hr and 77-90%, respectively. Reduction process is very effective, inexpensive and clean for synthesis of fluoroamines in good yield. The structures of the compounds are supported by FTIR, mass spectrometry ^1H and ^{13}C NMR spectral data.

Corresponding Authors
Fax: +912462250465
E-Mail: *dr.atshinde@gmail.com
[a] P.G. Department of Chemistry, N. E. S. Science College, Nanded(MS)-431605, India
[b] Department of Chemistry, M. P. College, Palam, Dist-Parbhani(MS)-431720
[c] P.G. Department of Chemistry, Yeshwant Mahavidyalaya Nanded (MS)-431602, India

Introduction

The chemistry of fluorine containing compounds has been tremendously developed. Intrinsic properties of fluorine atom, such as high electro negativity, small atomic radius, and low polarisability of the C-F bond, impart significant improvement on the biological activity of fluorinated molecules.[1] Fluorine has played pivotal role in novel drug discovery for modulating physical and biological properties of the molecules.[2-3] Thus, fluorine substitution remains an attractive means in the development of more active and selective pharmaceutical drug molecule.

Schiff bases constitute an area of rapidly growing interest because they form the basis of novel chemistry[4,5] interesting physical properties[6,7] and important biological activity.[8,9] Imines can be effectively reduced to amines by several reducing agents.[10-11] Sodium borohydride is a powerful reducing agents and has been employed in the reduction of a range of functional groups.[12,13] In the present work an effect has made to reduce some fluoro schif bases by $NaBH_4$, which is simple, safe and inexpensive reagent, and reduction can be achieved within 1-1.5 hrs.

Material and Methods

Instrumentation

Melting points were determined in an open capillary tube and are uncorrected. The chemicals and solvents were of laboratory grade and were purified. Completion of the reaction was monitored by thin layer chromatography using hexane/ethyl acetate as mobile phase on pre coated sheets of silica gel-G (Merck, Germany) using iodine vapor for detection. IR spectra recorded in KBr on a Perkin-Elmer spectrometer. ^1H and ^{13}C NMR (70MHz) spectra were recorded in DMSO-d_6 with an Avance spectrometer (Bruker, Germany) at 400-MHz frequency using TMS as an internal standard. The mass spectra were recorded on EISHIMADZU-GC/MS spectrometer. Elemental analyses were performed on a Perkin-Elmer 240 CHN elemental analyzer.

Synthesis

The reaction scheme for the reduction of fluoro Schiff bases is presented in **Scheme-1**. Into a 100mL flask 0.01 mole fluoro Schiff base (**1a-l**)[14] and 20mL MeOH were placed in an ice bath and 0.015 mole $NaBH_4$ was added pinch wise during 10 min. with stirring. After complete addition of $NaBH_4$, the reaction mixture was further stirred at RT for 1-1.5hr. The progress of the reaction was monitored by TLC. The solid separated on evaporation of solvent was filtered, washed with cold water and recrystalized from ethanol to get **2a-l.**

2-[(4-Fluorophenylamino)methyl]phenol (2a)

White solid, Yield 90 %, m.p.125 ^oC. IR KBr):3540 cm^{-1} (OH), 3248 cm^{-1} (NH), 2947 cm^{-1} (-CH). ^1H NMR (DMSO d_6): δ 4.01 (s, 1H, NH), δ 4.12 (s, 2H, -CH_2), δ 6.90-7.31 (m, 8H, Ar-H), δ 10.20 (s, 1H, Ar-OH); ^{13}C NMR; 156.2,153.1,145.3,143.4,136.1,134.3,130.7, 115.0, 113.6, 43.3. Anal Calcd for $C_{13}H_{12}FNO$ (217): C, 77.41; H, 5.52; N, 6.45. Found: C, 77.40; H, 5.31; N, 6.75

2,4-Dibromo-6-[(4-fluorophenylamino)methyl]phenol (2b)

Yellow solid, Yield 85 %, m.p.140 ^oC. IR (KBr):3550 cm^{-1} (OH), 3240 cm^{-1} (NH), 2930 cm^{-1} (-CH). ^1H NMR (DMSO d_6): δ 4.03 (s, 1H, NH), δ 4.20 (s, 2H, -CH_2), δ 6.90-7.31 (m, 6H, Ar-H), δ 10.30 (s, 1H, Ar-OH); ^{13}C NMR; δ 157.4, 154.2, 145.8, 144.1, 136.9, 132.6, 116.3, 114.6, 110.0, 105.6, 44.7. Anal Calcd for $C_{13}H_{10}Br_2FNO$ (374.18): C, 41.71; H, 2.67; N, 3.74. Found: C, 41.40; H, 2.31; N, 3.55.

4-Chloro-2-[(4-fluorophenylamino)methyl]phenol (2c)

White solid, yield 80 %, m.p. 120 ^oC. IR KBr): 3545cm^{-1} (OH), 3245cm^{-1}(NH), 2940cm^{-1}(-CH). ^1H NMR (DMSO d_6): δ 4.05 (s, 1H, NH), δ 4.20 (s, 2H, -CH_2), δ 7.00-7.45 (m, 7H,

Ar-H), δ 10.31 (s, 1H, Ar-OH); ^{13}C NMR; 158.4, 151.1, 144.1, 142.6, 137.0, 136.4, 130.7, 128.5, 115.3, 114.9, 43.3. Anal Calcd for $C_{13}H_{11}ClFNO$ (251.5): C, 62.00; H, 4.37; N, 5.30. Found: C, 62.02; H, 4.25; N, 5.30.

2-[(4-Fluorophenylamino)methyl]-2,6-diiodophenol (2d)

Yellow solid, Yield 85 %, m.p.110 ºC. IR (KBr):3535 cm^{-1} (OH), 3225 cm^{-1} (NH), 2915 cm^{-1} (-CH). ^{1}H NMR (DMSO d_6): δ 4.01 (s, 1H, NH), δ 4.13 (s, 2H, -CH_2), δ 6.85-7.25 (m, 6H, Ar-H), δ 10.12 (s, 1H, Ar-OH); ^{13}C NMR; δ 155.2, 152.3, 143.7, 142.1, 136.9, 131.0, 114.1, 111.6, 105.0, 102.9, 44.7. Anal Calcd for $C_{13}H_{10}F I_2NO$ (467): C, 32.26; H, 2.13; N, 2.99. Found: C, 32.55; H, 2.10; N, 3.01.

4-[(4-Fluorophenylamino)methyl]benzene-1,3-diol (2e)

White solid, Yield 85 %, m.p.135 ºC. IR KBr):3430 cm^{-1} (OH), 3235 cm^{-1} (NH), 2920 cm^{-1} (-CH). ^{1}H NMR (DMSO d_6): δ 4.05 (s, 1H, NH), δ 4.20 (s, 2H, -CH_2), δ 6.40-6.85 (m, 7H, Ar-H), δ 10.01 (s, 2H, 2Ar-OH); ^{13}C NMR; 158.0, 156.1, 143.4, 140.7, 137.0, 130.2, 115.3, 114.9, 110.0, 105.8, 43.3. Anal Calcd for $C_{13}H_{12}FNO_2$ (233): C, 66.95; H, 5.15; N, 6.00. Found: C, 67.02; H, 5.10; N, 6.05.

2-Ethoxy-4-[(4-fluorophenylamino)methyl]phenol (2f)

White solid, Yield 85 %, m.p.148 ºC. IR KBr): 3510 cm^{-1} (OH), 3240 cm^{-1} (NH), 2890 cm^{-1} (-CH). ^{1}H NMR (DMSO d_6): δ1.35 (t, 3H, CH_3) δ3.90 (q, 2H, CH_2), δ 4.13 (s, 1H, NH), δ 4.20 (s, 2H, -CH_2), δ 7.10-7.90 (m, 7H, Ar-H), δ 10.01 (s, 1H, Ar-OH); ^{13}C NMR; 158.3, 156.1, 150.8, 134.7, 133.5, 130.0, 123.6, 116.5, 112.3, 114.9, 65.2, 56.4, 18.0. Anal Calcd for $C_{15}H_{16}FNO_2$ (261): C, 68.96; H, 6.13; N, 5.36. Found: C, 68.56; H, 6.05; N, 5.45.

2-Bromo-6-ethoxy-4-[(4-fluorophenylamino)methyl]phenol (2g)

Brown solid, Yield 85 %, m.p.152 ºC. IR KBr):3515 cm^{-1} (OH), 3252 cm^{-1} (NH), 2920 cm^{-1} (-CH). ^{1}H NMR (DMSO d_6): δ1.37 (t, 3H, CH_3) δ3.96 (q, 2H, CH_2), δ 4.09 (s, 1H, NH), δ 4.15 (s, 2H, -CH_2), δ 7.15-7.95 (m, 6H, Ar-H), δ 10.10 (s, 1H, Ar-OH); ^{13}C NMR; 158.7, 156.1, 151.0, 135.2, 134.1, 131.0, 124.5, 117.2, 113.3, 115.0, 65.8, 56.9, 18.8. Anal Calcd for $C_{15}H_{15}BrFNO_2$ (339.5): C, 53.01; H, 4.41; N, 4.12. Found: C, 53.00; H, 4.35; N, 4.20.

2-Ethoxy-4-[(4-fluorophenylamino)methyl]-6-iodophenol (2h)

Yellow solid, yield 77 %, m.p.135 ºC. IR KBr):3505 cm^{-1} (OH), 3210 cm^{-1} (NH), 2910 cm^{-1} (-CH). ^{1}H NMR (DMSO d_6): δ1.30 (t, 3H, CH_3) δ3.85 (q, 2H, CH_2), δ 4.10 (s, 1H, NH), δ 4.15 (s, 2H, -CH_2), δ 7.09-7.80 (m, 7H, Ar-H), δ 10.03 (s, 1H, Ar-OH); ^{13}C NMR; 158.1, 156.1, 149.8, 134.3, 133.0, 130.7, 122.9, 117.1, 111.8, 113.2, 64.1, 56.1, 18.0. Anal Calcd for $C_{15}H_{15}FINO_2$ (387): C, 46.51; H, 3.87; N, 3.61. Found: C, 46.70; H, 3.05; N, 3.80.

4-[(4-Fluorophenylamino)methyl]-2-methoxyphenol (2i)

White solid, Yield 85 %, m.p. 141 ºC. IR KBr): 3510 cm^{-1} (OH), 3260 cm^{-1} (NH), 2925 cm^{-1} (-CH). ^{1}H NMR (DMSO d_6): δ 3.70(s, 3H, CH_3) δ 4.22 (s, 1H, NH), δ 4.32 (s, 2H, -CH_2), δ 6.40-6.80 (m, 7H, Ar-H), δ 10.05 (s, 1H, Ar-OH); ^{13}C NMR; 158.5, 153.0, 145.1, 139.1, 136.0, 120.8, 116.8, 115.9, 114.3, 113.9, 61.2, 46.2. Anal Calcd for $C_{14}H_{14}FNO_2$ (247): C, 68.01; H, 5.66; N, 5.67. Found: C, 68.10; H, 5.75; N, 5.70.

2-Bromo-4-[(4-fluorophenylamino)methyl]-6-methoxyphenol (2j)

Faint yellow solid, yield 80 %, m.p.145 ºC. IR KBr):3513 cm^{-1} (OH), 3275 cm^{-1} (NH), 2940 cm^{-1} (-CH). ^{1}H NMR (DMSO d_6): δ3.80(s, 3H, CH_3) δ 4.25 (s, 1H, NH), δ 4.36 (s, 2H, -CH_2), δ 6.45-6.90 (m, 6H, Ar-H), δ 10.10 (s, 1H, Ar-OH); ^{13}C NMR; 158.7, 153.3, 145.5, 139.2, 136.6, 121.0, 117.1, 116.0, 114.7, 114.3, 61.8, 44.1. Anal Calcd for $C_{14}H_{13}BrFNO_2$ (325.5): C, 51.61; H, 3.99; N, 4.30. Found: C, 51.40; H, 4.01; N, 4.25.

2-Chloro-4-[(4-fluorophenylamino)methyl]-6-methoxyphenol (2k)

White solid, Yield 78 %, m.p. 138 ºC. IR KBr):3515 cm^{-1} (OH), 3265 cm^{-1} (NH), 2940 cm^{-1} (-CH). ^{1}H NMR (DMSO d_6): δ3.75(s, 3H, CH_3) δ 4.3 (s, 1H, NH), δ 4.40 (s, 2H, -CH_2), δ 6.50-7.00 (m, 6H, Ar-H), δ 10.16 (s, 1H, Ar-OH); ^{13}C NMR; 159.1, 153.8, 146.0, 139.7, 137.3, 121.8, 117.7, 117.1, 115.0, 114.9, 62.0, 44.5. Anal Calcd for $C_{14}H_{13}ClFNO_2$ (281.5): C, 59.68; H, 4.61; N, 4.97. Found: C, 59.40; H, 4.72; N, 4.60

4-[(4-Fluorophenylamino)methyl]-2-iodo-6-methoxyphenol (2l)

Yellow solid, Yield 77 %, m.p. 130 ºC. IR KBr):3500 cm^{-1} (OH), 3215 cm^{-1} (NH), 2904 cm^{-1} (-CH). ^{1}H NMR (DMSO d_6): δ 3.80(s, 3H, CH_3) δ 4.17 (s, 1H, NH), δ 4.20 (s, 2H, -CH_2), δ 6.55-7.10 (m, 6H, Ar-H), δ 10.10 (s, 1H, Ar-OH); ^{13}C NMR; 159.0, 153.2, 145.8, 137.1, 137.0, 121.5, 116.6, 116.3, 114.4, 114.0, 62.5, 44.0. Anal Calcd for $C_{14}H_{13}FINO_2$ (373): C, 5.01; H, 3.48; N, 3.75. Found: C, 45.51; H, 3.62; N, 3.50

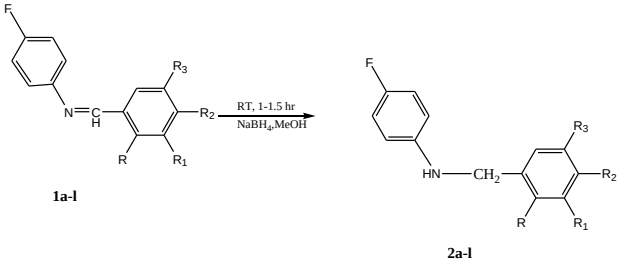

1a-l **2a-l**

1a, 2a: R=OH; R_1, R_2, R_3=H; **1b, 2b**: R=OH; R_1, R_3=Br, R_2=H; **1c, 2c:** R=OH; R_1, R_2=H, R_3=Cl; **1d, 2d**: R=OH; R_1, R_3=I, R_2=H; **1e, 2e:** R, R_2=OH; R_1, R_2=H; **1f, 2f:** R, R_3=H; R_1=OEt, R_2=OH; **1g, 2g**: R=H; R_1=OEt; R_2=OH; R_3=Br **1h, 2h**: R=H; R_1=OEt; R_2=OH; R_3=I; **1i, 2i**: R, R_3=H; R_1=OMe, R_2=OH; **1j, 2j**: R=H; R_1=OMe, R_2=OH, R_3=Br; **1k, 2k:** R=H; R_1=OMe, R_2=OH, R_3=Cl; 1l, 2l: R=H; R_1=OMe, R_2=OH

Scheme1. Reduction of fluoroimines.

Results and discussion

This paper describes very simple methodologies developed for effective reduction of fluoro schif bases using sodium borohydride as a reducing agent. Similar methodologies have been found effective in reducing ketones to alcohols in an aprotic solvents[15]. Several structurally varied Schiff bases underwent reduction by this procedure to produce the corresponding secondary amines in high yields[16,19]. Sodium borohydride thus appears to be very efficient reagent for the reduction of imines to the corresponding amines in high yields. Moreover, the easy availability of reagent, operational simplicity and generality makes this procedure extremely attractive. The procedure does not require anhydrous condition is inexpensive and avoids the use of inert atmosphere.

Conclusion

We have described a convenient procedure by means of $NaBH_4$ has shown to convert fluoro imines into corresponding amines. The structures of all the amines are supported by FTIR, ^1H and ^{13}C NMR and mass spectroscopic techniques. The developed method is simple, inexpensive and safe for the one-pot reduction of imines.

Acknowledgements

The authors are thankful to Principal, N.E.S. Science College, Nanded for providing laboratory facilities and Director Indian Institute of Chemical Technology (IICT), Hyderabad, for providing necessary instrumental facilities.

References

[1]Joshi, K.C., Dandia, A., Khanna, S., *Indian J. Chem*., **1990**, *29*B, 1125-1128.

[2]Muller, K., Faeh, C., Diederich, C., *Science*, **2007**, *317*, 1881-1886.

[3]Ismail, F.M.D., *J. Fluorine Chem*., **2002**, *118*, 27-33.

[4]Syamal, A., Maurya, M. R., *Coord. Chem. Rev*., **1989**, *95*, 183-238.

[5]Gibson, V. C., Spitzmesser, S. K., *Chem. Rev*., **2003**, *103*, 283-315.

[6]Marcos, M., Serrano, J. L., Sierra, T., *Chem. Mater*., **1993**, *5*, 1332-1337

[7]Ghedani, M., Pucci, D., Cesarotti, E., Francescangeli, O., Bartolino, R., *Liq. Cryst*., **1993**, *15*, 331-344.

[8]Shinde, A., Zangade, S., Chavan, S., Vibhute, Y., *Org. Commun*., **2014**, *7(2)*, 60-67

[9]Chan, A .S., Chen,C. C., Lin, C. W., Cheng, M. C., Peng, S. M., *Chem. Commun*., **1995**, *17*, 1767-1768.

[10]a)Emerson, W. S., *The preparation of amines by reductive Alkylation, Org. Reactions*, Vol.4, Wiley & Sons, **1978**.b) Friefelder, M., *Catalytic hydrogenation in organic synthesis. Procedures and Commentry*, Wiley & Sons, **1978**. c) Speckenbach, B., Bisel, P., Frahm, A. W., *Synthesis*, **1977**, *11*, 1325-1331.

[11]a)Billman, J. H., Tai, K. M., *J. Org. Chem*., **1958**, *23*, 535-539 b) Billman, J. H., Diesing, .C., J. *Org. Chem*., **1957**, *22*, 1068-1070 c) De Savignac, M. A., Bon, M., Mazarguil, H., Latters, A., *Bull. Chim. Soc. Fr*., **1975(**9-10), 2075-2073 d) Wrobel, J. E., Ganem, B., *Tetrahedron Lett*., **1981**, *22*, 3447-3450 e) Hutchins, R. O., Su, W. Y., *Tetrahedron Lett*., 1984, *25*, 695-698 f) Cho, B. T., Chun, Y. S., *Tetrahedron Asymmetry*., **1992**, *3*, 1583-1590

[12]Tsukinoki, T., Mitoma, Y., Nagashima, S., Kawaji, T., Hushimoto, I., Tashino, M., *Tetrahedron Lett.*, **1998**, *39*, 8873-8876

[13]Periasamy, M., deasagayaraj, A., Satyanarayana, N., Narayana, C., *Synth. Commun*., **1989**, *19*, 565-573

[14]Shinde, A. T., Zangade, S. B., Chavan, S. B., Vibhute, Y. B., *Am. J. Pharm. Tech. Res*., **2011**, *1*, 43-48.

[15]Yakabe, S., Hirano, M., Marimoto, T., *Synth. Commun*., **1999**, 29, 295-302

[16]Yalcin, B., Medsidov, A. A., Nasrullayeva, T. M., Tascioglu, S., Aydin, A., *Indian. J. Chem*., **2008**, *47*B, 699-704

[17]Aghera, V. K., Persania, H. P., *Indian J. Chem*., **2009**, *48*B, 438-442

[18]Zito, S. W., Martinez, C. M., *J. Biol. Chem*., **1980**, *255*, 8645-8649

[19]Pandilov, A. V., Markovich, Y. D., Ivashev, T. P., Zhirov, A. A., Ellev, A. F., kurochkin, V. K., Kirsanov, A. T., Nazarov, G. V., *Pharm. Chem. J*., **2000**, *34*, 32-33.

Received: 15.11.2015.
Accepted: 07.02.2016.

PREDICTION OF VAPOUR-LIQUID EQUILIBRIUM FOR n-ALKANE FLUIDS

B. P. Akhouri,[a]* K. Akhtar[b] and T. P. Akhouri[b]

Keywords: equations of state; vapour liquid equilibrium; critical parameters; hard convex body chain.

Analysis of the equations of state of the hard convex body chain and hard spheres has been done for predicting the vapor liquid equilibrium (VLE) of simple fluids of n-alkanes. The repulsive part of the Boublik equation of state for the hard convex body chain has been found as an equivalent alternative either for the well known Carnahan-Starling repulsive term or the established van der Waals repulsive part of hard spheres equations of state. The attractive parts of these equations of state have the similar form as that of the van der Waals and are obeying the power-law temperature dependency. Add-on separation method of compressibility factor has been used for these equations of state. The simulated data for VLE densities from these equations of state are found to agree well with the available experimental data for n-alkane fluids.

* Corresponding Authors
E-Mail: binayakhouri@yahoo.in
[a] Department of Physics, Birsa college, Khunti-835210, Jharkhand, India.
[b] Post Graduate Department of Chemistry, Ranchi College, Ranchi-834008, Jharkhand, India.

Introduction

An equation of state (EoS) is an analytical expression relating pressure to the volume and temperature. The expression of an equation of state is used[1-3] to describe the volumetric behavior, the VLE and the thermal properties of pure substances and mixtures. Numerous EoS have been proposed to represent the phase behavior of pure substances and mixtures in the gas and liquid states since van der Waals introduced his expression in 1873. The van der Waals equation provides a qualitatively correct description of the critical point and VLE envelope but for practical applications it is very crude. Nonetheless, it formed a certain basis for developing dozens of empirical EoS used in engineering applications.[4-6]

The attraction parameter *a* of van der Waals needed to be made a function of temperature before any cubic EoS was able to do a better job of quantitatively matching experimental data. This was a realization that van der Waals himself had suggested, but no actual functional dependency had been introduced until the Redlich-Kwong[5] EoS. The Redlich-Kong EoS improved the accuracy of the van der Waals by proposing a temperature dependence attractive term. Thus, the compressibility factors of most empirical equations of state can be expressed as the sum of a temperature-independent term and a temperature-dependent term. Using this functional dependency of temperature in attractive term, the improvement in results for the VLE properties is found significant when the simple but very precise Carnahan–Starling equation has been used. Since these EoS are cubic in volume, so that the van der Waals concept is retained.

Molecular simulation reveals that the inaccuracies of attractive and repulsive terms respond to some disadvantages to the use of cubic equations of state, and these inaccuracies are cancelled by one other when the EoS's are employed for the calculation of fluid properties, specifically for the VLE densities. Researchers has emphasized considerably on modeling of long and convex molecules in addition to modeling of small and simple molecules. Based on theory of Prigogine[7] and Flory,[8] an equation for molecules, treating them as chains of segments, which is called Perturbed-Hard-Chain–theory (PHCT), was expressed by Beret and Prausnitz,[9] Donohue and Prausnitz[10] and by Gross and Sadowski.[11] Large non-spherical molecules such as heavy hydrocarbons and polymers are theoretically modeled as chain like molecules. A chain of tangent hard spheres is the simplest model of this type of molecule. Relaxation of tangency constraint in the tangent hard sphere chains by allowing adjacent hard spheres along the chain to overlap leads to a more realistic model which is known as fused hard sphere chain.

Conversely, in the limit, when the center to center reduced length tends to one, the EoS for a fused hard sphere chain reduce to an equation of state of thermodynamic perturbation theory for a tangent hard sphere chain.[12]

We have considered different forms for the repulsive part for equations of state[13] of hard spheres such as vdW EoS or CSvdW EoS[14,15] and also for the equation of state of hard convex body chains such as Boublik[16,17] vdW EoS. For the attractive part of these EoS, we have considered the exponent term to the temperature to zero to reproduce the usual form of vdW or CSvdW or Boublik vdW EoS. In this article, the chemical potential for Boublik vdW EoS has been derived and used to predict the VLE densities of n-alkane fluids. The predictions corresponding to this group of EoS are within a degree of quality similar to the widely used Carnahan-Starling equation.

Equations of state for HS and HCB fluids

This section includes three groups of equations of state. The three groups are made on the basis of extensively used add-on separation method of compressibility factor[19-23] as $Z = Z_{rep} + Z_{att}$. The functional dependency of temperature, as introduced by Redlich and Kwong[5], has a power-law form $T^{-\delta}$ for the attractive part of the EoS. For the expression of repulsive part of the EoS has any of the three forms i.e. of vdW, CS and Boublik . It may be noted that in all calculations we set up a new parameter δ as the temperature-exponent in the attractive term. Also that the selection to set up δ = 0 regains the original EoS. The critical parameters and the analytic expressions for the chemical potential have been determined for the three groups, which allowed us to obtain the VLE densities. Here, for simplicity in calculation we employed the dimensionless variable $y = b/4v$ in place of the molar volume, ν with b being the co-volume. Here, $y = b/4v$ is known as packing fraction.[20-23]

As is well known, the chemical potential, μ, can be analytically obtained through Eqn 1.[13]

$$\mu = \int \frac{b}{4y}\left(\frac{\partial P}{\partial y}\right)_T dy + \varphi(T) \qquad (1)$$

where, the function φ has the temperature dependency. The compressibility factor is expressed as Eqn. 2.

$$Z = \frac{bP}{4yRT} \qquad (2)$$

where R is the molar universal gas constant.

To obtain an analytical expression for μ from Eqn. 1, one requires an analytic expression for the EoS.

The van der Waals (vdW-δ) groups

The compressibility factor for the vdW-δ set of EoS is written as Eqn. 3.

$$Z = \frac{1}{1-4y} - \frac{4ay}{bRT^{1+\delta}} \qquad (3)$$

For δ = 0, Eqn. 3 reproduces the vdW EoS. The critical point conditions can be solved to yield the critical parameters: y_c=0.083333, Z_c=0.375 and

$$a = \lambda b R T_c^{1+\delta}, \qquad (4)$$

where λ = 3.375.

Using eqn. 1, the expression obtained for chemical potential is given by eqn. 5.

$$\mu(y,T) = \frac{RT}{1-4y} - \frac{8ay}{bT^{\delta}} + RT\log\left|-\frac{y}{1-4y}\right| + \varphi(T), \qquad (5)$$

The Carnahan-Starling-van der Waals (CSvdW-δ) group

The CSvdW-δ group assumes its form by replacing the classical vdW repulsive term in eqn. 3 with the CS hard sphere EoS. The functional dependency of temperature for the attractive term of the EoS remains unchanged as in Eqn. 3. The compressibility factor for CS vdW-δ EoS can now be written as

$$Z = \frac{1+y+y^2-y^3}{(1-y)^3} - \frac{4ay}{bRT^{1+\delta}} \qquad (6)$$

For δ = 0, Eqn. 6 reproduces the usual form of the CSvdW EoS.[15]

Using eqn. 1, the expression obtained for chemical potential is given by eqn. 7.

$$\mu(y,T) = \frac{RT(3-y)}{(1-y)^3} - \frac{8ay}{bT^{\delta}} + RT\log(y) + \varphi(T) \qquad (7)$$

The Boublik- van der Waals (Boublik vdW-δ) group

Boublik proposed an equation (eqn. 8) of state for Hard Convex Bodies.[16]

$$Z_{hcb} = \frac{1+(3\alpha-2)y+(3\alpha^2-3\alpha+1)y^2-\alpha^2y^3}{(1-y)^3} - \frac{4ay}{bRT^{1+\delta}} \qquad (8)$$

where, α is the non-sphericity parameter. When, α = 1 , Eqn. 8 reduces to Carnahan Starling equation. For, other hard convex body, α > 1. According to Boublik et al,[17] the hard convex body equation can be extended to hard chain molecules of overlapping hard spheres ($0.5 < L < 1$) or tangent hard spheres (L=1) with formulation of parameter of non-spherecity as Eqn. 9.

$$\alpha = \frac{[1+(m-1)L][2+(m-1)L]}{2+(m-1)(3L-L^3)} \qquad (9)$$

Using Eqn. 1, the expression obtained for chemical potential is given by Eqn. 10.

$$\mu(y,T)=\frac{RT\left(y^2-2y+1\right)}{\left(1-y\right)^3}-\frac{\alpha^2RT\left(y^2-4y+1\right)}{\left(1-y\right)^3}- \tag{10}$$

$$\frac{3\alpha RT\left(y-1\right)}{\left(1-y\right)^3}-\frac{8ay}{bT^{\delta}}+RT\left(1-\alpha^2\right)\log\left(1-y\right)+$$

$$RT\log\left(y\right)+\varphi(T)$$

For α=1, Eqn. (10) represents the same equation for the chemical potential as that of the CS EoS.

The non-sphericity of the molecule is modeled in terms of the *m*-segments of hard convex bodies. It forms a hard molecule with a chain of freely jointed hard convex bodies. Each n-alkane can be modeled as a chain of *m* segments of hard HCB. For determination of *m*-segment value for each n-alkane, one should comprehend that there should be some fundamental phial of our couch of m based on the nature of the HCB. For example, pentane is structured as $CH_3CH_2CH_2CH_3$. One may accept that the base unit for pentane is CH_2CH_2, which could be approximately modelled as ethane (CH_3CH_3). Since, two atoms of carbon cannot be approximated as one atom of carbon because of its higher mass as compared to the mass of hydrogen. But for lighter hydrogen one can approximate two hydrogen atoms as one atom or vice versa. Knowing the HCB of ethane and using this base of HCB with *m* = 2.5 to model Pentane. For decane, using the CH_2CH_2 as HCB, *m* = 5. Note that the values guarded by the base model for the HCB have only sense in modelling the n-alkanes. Using this concept, the value of *m* has been calculated for each n-alkane and is tabulated in Table 1. The table also gives the values of the non-sphericity parameter α as calculated using Eqn. (9).

For n-alkanes, when δ = 0, the critical point conditions can be solved to yield the critical parameters. The calculated critical parameters for pressure, temperature and volume for selected n-alkanes are:

Ethane

$$P_{cr}=\frac{1.20137\alpha}{17b^2};\quad T_{cr}=\frac{6.41435\alpha}{17bR}\quad V_{cr}=1.91653b$$

Hexane

$$P_{cr}=\frac{364.365\alpha}{17b^2};\quad T_{cr}=\frac{2879.92\alpha}{12197bR}\quad V_{cr}=2.78929b$$

Decane

$$P_{cr}=\frac{483.575\alpha}{28863b^2};\quad T_{cr}=\frac{4993.44\alpha}{28863bR}\quad V_{cr}=3.6077b$$

Results and discussion

We examined the behavior of the three groups of EoS's by calculating the VLE densities, and compared them with the experimental data[18] for fluids of n-alkanes. In particular, we calculated the co-existence curves in the y_r versus T_r diagram. The calculations were made by taking δ=0 and 0.7 that we had observed to include the best choice for comparison with real data. Figures 1-3 represent the results for the VLE densities (in reduced units) versus the reduced temperatures. The points represent the experimental data for n-alkanes (ethane, hexane and pentane) fluids,[18] and the lines represent the predictions obtained with the vdW-δ, Boublik vdW-δ groups of EoS's.

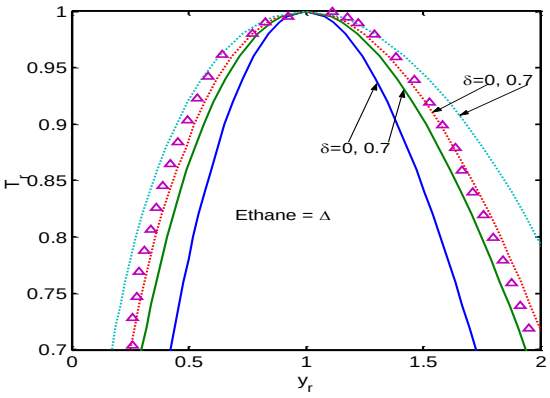

Figure 1. Plot of the reduced temperature versus reduced density for the VLE of ethane.

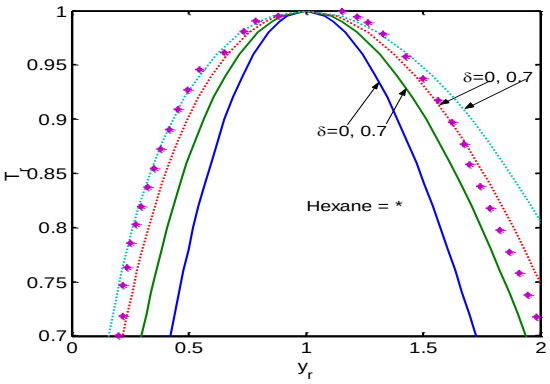

Figure 2. Plot of the reduced temperature *versus* reduced density for the VLE of hexane.

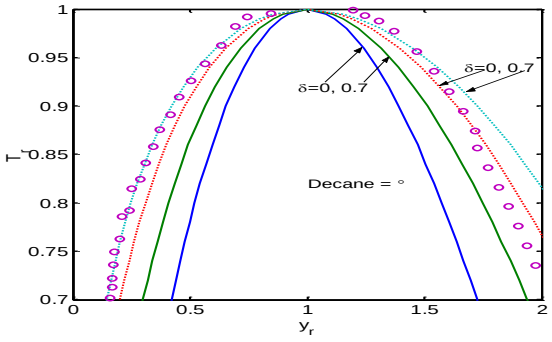

Figure 3. Plot of the reduced temperature *versus* reduced density for the VLE of decane.

Table 1. Values of the critical and the nonsphericity parameter for a given HCB segment *m*.

Alkane	*m*	α	y_c	Z_c	λ
Ethane	1	1	0.13044408	0.352899	4.235187
Pentane	3.0	1.75			
Hexane	3.0	2	0.08962854	0.352899	4.235187
Heptane	3.5	2.25			
Octane	4.0	2.5			
Nonane	4.5	2.75			
Decane	5.0	3	0.0692945	0.349386	5.780184

It may be noted that Figures 1-3 have been drawn separately for clear representation of the data lines and the available experimental points of selected n-alkanes. Figure 4 simply represents all the three figures (1)-(3) together in order to get a close difference between them. In Figures 1-3, the continuous lines represent the groups belonging to the classical vdW-δ repulsive term and the dotted lines represent the groups belonging to the Boublik repulsive term. In figure 1, note that the dotted lines reproduce the data for CS EoS for m=1 and α=1. Figure 4 represents co-existence curves in the Y_r versus T_r diagram with the EoS's for the values of exponent δ = 0, 0.7 and the experimental points of the VLE densities for selected n-alkane fluids. In Figure 4, for representing lines for exponent δ = 0, 0.7 continuous lines are used (classical vdW-δ).

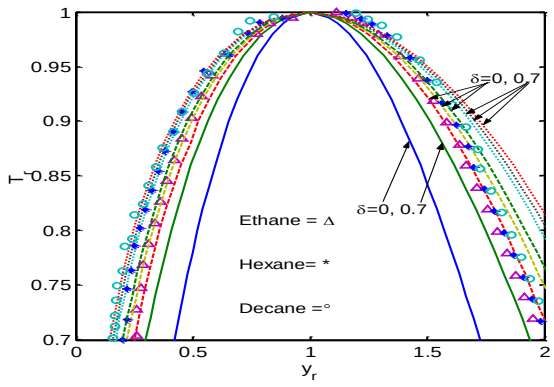

Figure 4. Plot of the reduced temperature *versus* reduced density for the VLE. The symbols represent data for Ethane, Hexane and Decane.

For Boublik vdW-δ, the lines for exponent δ =0 are represented by dashed lines and the lines for exponent δ = 0.7 are represented by dotted lines. From these observations it is clear that the modifications to temperature dependence i.e., by varying the exponentδ of the attraction term improve the result of prediction of saturation densities.

However, the co-existence curves of figure 4 shows that the saturation densities calculated with the classical vdW EoS (δ=0) are unsatisfactory. From the analysis of these coexistence curves it is evident that the use of CS EoS for the repulsive term only improves the results on the liquid branch over a small range of temperature. However, the plot of the theoretical liquid saturation densities is certainly different from that of the experimental points corresponding to both branches of the co-existence curve. It is clear that, by taking the several δ exponents in the CS vdW EoS or Boublik vdW-δ, one can observe both the liquid and vapour branches in good correspondence with the experimental points for fluids, but this is deviational for the case of the classical vdW-δ groups. We conclude from this result that for each vdW-δ of EoS's group there must be a best value for the exponent δ for each fluid. Our study for simple fluids of n-alkanes, we may consider the best value to be in the range (0-1).

Conclusions

In this article, equations for chemical potential have been derived. These equations have been utilized in finding the VLE density of HCB chain and HS systems. All the three groups of EoS[24-30] have been studied by finding the VLE densities of n-alkane fluids. The observations clearly indicates that the EoS obtained by add-on separation method of compressibility factor[20,21] as $Z = Z_{rep} + Z_{att}$, have predicted the experimental data closely. The predictions of VLE densities for these fluids can be numerically improved by finding the best value of the δ exponent for each case. The better results in the work related to mixtures and mixing rules can be obtained if a most suitable choice for the δ-exponent value becomes available.

Acknowledgements

One of us (B.P.A) specially thanks the University Grant Commission, Government of India for financial support (PSJ-001/13-14).

References

[1]Yelash, L. V., and Kraska, T., *Fluid Phase Equil.*, **1999**, *162*, 115-130.

[2]Valderrama, J. O., *Ind. Eng. Chem. Res.*, **2003**, *42*, 1603-1618.

[3]Wei, Y. S., Sadus, R. J., *AIChE J.*, **2000**, *46(1)*, 169-196.

[4]Esmaeilzadeh, F., Roshanfeker, M., *Fluid Phase Equil.*, **2006**, *239*, 83-90.

[5]Redlich, O., Kwong, J. N. S., *Chem. Rev.*, **1949,** *44*, 233-244.

[6]Bertacco, A., Elvassore, N., Fermeglia, M., Prausnitz, J. M., *Fluid Phase Equil.*, **1999**, *158*,183–191.

[7]Prigogine, I. *The Molecular Theory of Solutions*, **1957**, North-Holland, Amsterdam.

[8]Flory, P. J., *J. Am. Chem. Soc.*, **1965**, *87*, 1833-1838.

[9]Abrams, D. S., Praunitz, J. M., *AIChE J.*, **1975**, *21*,116-128.

[10]Donohue, M. D., Prausnitz, J. M., *AIChE J.*, **1978**, *24(5)*, 849-860.

[11]Gross, J., Sadowski, G., *Ind. Eng. Chem.Res.*, **2001**,*40(4)*,1244-1260.

[12]Waziri, S. M., Hamad, E. Z., *Ind. Eng. Chem. Res.*, **2008**, *47*, 9658-9662.

[13]Roma´n, F. L., Mulero, A., F., Cuadros, F., *Phys . Chem. Chem. Phys.*, **2004**, *6*, 5402 – 5409.

[14]Carnahan, N. F., Starling, K. E., *AIChE J.*, **1972**, *18*, 1184-1189.

[15]Carnahan, N. F., Starling, K. E., *J. Chem. Phys.*, **1969**, *51*, 635-636.

[16]Boublik, T., *J. Chem. Phys.*, **1975**, *63*, 4084-4085.

[17]Boublik, T., Vega, C., Pena, M. D., *J. Chem. Phys.*, **1990**, *93*,730-736.

[18]Lemmon, E. W., McLinden, M. O., Fiend, D. G., Thermophysical Properties of Fluid Systems in NIST Chemistry WebBook, *NIST Standard Reference Database* n. 69, ed. Linstrom, P.J. Mallard, W.G., National Institute of Standards and Technology (NIST), Gaithersburg, M.D., http://webbook.nist.gov.

[19]Sadus, R. J., *J. Chem. Phys*., **2001**, *115*, 1460-1462.

[20]Sadus, R. J., *J. Chem. Phys.*, **2002**,*116*, 5913-5913.

[21]Sadus, R. J., *Phys. Chem. Chem. Phys*., **2002**, *4*, 919-921.

[22]Peng, D. Y., Robinson, D. B., *Ind. Eng. Chem. Fundam.*, **1976**, *15*, 59-64.

[23]Mathias, P. M., Naheiri, T., Oh, E. M., *Fluid Phase Equil*., **1989**, *47*, 77-87.

[24]Song, Y., Hino,T., Lambert, S. M., Prausnitz, J. M., *Fluid Phase Equil*., **1996**, *117*, 69-76.

[25]Mulia, K., Yesavage,V. F., *Fluid Phase Equil.*, **1989**, *52*, 67–74.

[26]Walsh, J. M., Gubbins, K. E., *J. Phys. Chem.*, **1990**, *94*, 5115–5120.

[27]Mohsen-Nia, M., Modarressa, H., Mansoori, G. A., *Fluid Phase Equil.*, **2003**, *206*, 27-39.

[28]Mathias, P. M., *Ind. Eng. Chem. Res.*, **2003**, *42*, 7037-7044.

[29]Wang, H. T., Tasi, J. C., Chen, Y. P., *Fluid Phase Equil.*, **1997**, *138*, 43-59.

[30]Bertacco, A., Elvassore, N., Fermeglia, M., Prausnitz, J. M., *Fluid Phase Equilib.*, **1999**, *158*, 183-191.

Received: 12.12.2015.
Accepted: 07.02.2016.

SATURATION AND WETTABILITY EVOLUTION UNDER NON-ISOTHERMAL CARBON DIOXIDE INJECTION INTO SALINE AQUIFER

Adango Miadonye[a] and Mumuni Amadu[b]

Keywords: wettability; saturation; shear failure; CO_2 injection; geosequestration; diffusivity; thermophysical; steady state.

To reduce the cost of carbon capture, transportation and eventual geologic storage at potential geologic sites future sequestration plans envisage the locating of power plants at potential geologic sites. The implication is that the injection temperature of flue gas will be typically those encountered in combustion power plants. This, obviously has a geomechanical consequence considering the fact that heat transferred from the aquifer to the low permeability cap rock will cause excessive pore pressure build up due to poor pore pressure diffusion characteristics of these rocks. While these low permeability rocks are required to provide stratigraphic trapping mechanisms such excessive pore pressure build up can result in compromising the geomechanical integrity. This paper has used heat transfer theories and geomechanical concepts to obtain steady state temperature distribution in cap rocks for temperatures ranging from 50 to 800 °C. In so doing, cap rock critical temperatures for tensile and shear failures have been established for a potential on-site gas injection into saline aquifers.

* Corresponding Authors
E-Mail: adango_miadonye@cbu.ca
[a] Department of Chemistry, Cape Breton University, P.O. Box 5300, Sydney, NS, Canada.
[b] Department of Process Engineering and Applied Science, Dalhousie University, Halifax, NS, Canada

Introduction

The main global warming due to anthropogenic emission of carbon dioxide is an issue that has captured global attention in both scientific and political debates and will continue to do so in this century if society needs to build a culture free from ecologic disaster similar to that suffered by the Maya civilization.[1,2] The Maya was a Mesoamerican civilization (2000 BC-250 AD) that attained a well-documented peak and glory until adverse climate change totally decimated its glorious achievements.[1] The current dramatic increase in the level of carbon dioxide has resulted from emissions at record levels due to a number of anthropogenic causes notably the burning of fossil fuels for power generation, industrial activities related to ammonium sulphate and cement production, gas processing, and other subordinate sources of emissions such as road and aviation transportation activities. To decarbonize the global economy requires the capture and storage of carbon dioxide. Internationally a number of geologically acceptable storage options have been proposed. They are depleted oil and gas reservoir, saline aquifers, thin coal seams, salt caverns as well as an ocean storage option. By considering the geographical distributions and availability coupled with techno-economic information, sequestration in saline aquifers appear most attractive on the basis of both global availability and global storage capacity.

The aim of this paper is to address the theoretical aspect of the problem and this will consist of modelling heat transfer in the injection interval and coupling of temperature field solution with petrophysical concepts. Classical texts dealing with two phase flow have always tackled the problem of saturation evolution under non-isothermal conditions. There are limited to none existence of published report of laboratory data on relative permeability or fluid saturation under non-isothermal conditions. In the light of supercritical carbon dioxide entering the saline aquifer and flowing under non-isothermal conditions it is the objective of this paper to address the problem of fluid saturation and wettability evolution under temperature gradient or non-isothermal conditions. This work has been motivated from the fact that the petrophysical flow functions notably fluid saturations, capillary pressure and the state of wettability of the porous medium are functions of temperature. These, therefore, will evolve under temperature gradient, and knowledge of them are essential in predicting the hydrodynamics of immiscible two phase flow involving supercritical carbon dioxide and resident formation brine.

Mathematical Development of the Problem

The injection of supercritical carbon dioxide into a deep saline aquifer for a long term geological storage involves a coupled thermal and hydrologic process, the principles of which are the underlying fundamental principles of thermo-poroelasticity. This involves combined principles of Darcy flow in porous media, hooks low of elasticity and thermal effect applied to a fluid containing porous body. Under conditions of non-isothermal flow the temperature field of the system will govern mechanical deformations. However, the thermo-poroelastic coupling coefficient defined as the ratio of the thermal energy stored in the system for a given temperature change to that stored in the system due to mechanical deformation has been found to be negligible for most rock systems.[3] Consequently in solving for the temperature field the problem can be decoupled such that the temperature field can be modelled and solve without due regard to the deformation field. Furthermore, since pressure or hydraulic is far higher than thermal diffusivity it will be assumed that the temperature field is not strongly coupled to the pressure field. The

problem formulation approach of this paper will therefore adopt the decoupling approach that has been reported in the literature of geomechanics.[4]

The injection of heat energy contained in a fluid into a porous water saturated medium consisting of a void space and solid matrix can be described by an energy balance equation. If the solid matrix and fluid are regarded as two pseudo-continua where the averaged solid temperature and the averaged fluid temperature represent the local thermal state of each phase the energy balance equation reads:[5]

$$\phi C_{\mathrm{f}} \frac{\partial T_{\mathrm{f}}(r,t)}{\partial t} + C_{\mathrm{f}} U_{\mathrm{f}} \frac{\partial T_{\mathrm{f}}}{\partial r} = -\frac{\partial q_{\mathrm{f}}(r,t)}{\partial r} - hA_{\mathrm{p}} a_{\mathrm{c}} \left(T_{\mathrm{s}} - T_{\mathrm{f}}\right) \tag{1}$$

for the fluid

$$(1-\phi) C_{\mathrm{s}} \frac{\partial T_{\mathrm{s}}(r,t)}{\partial t} + C_{\mathrm{s}} U_{\mathrm{s}} \frac{\partial T_{\mathrm{s}}}{\partial r} = -\frac{\partial q_{\mathrm{s}}(r,t)}{\partial r} + hA_{\mathrm{p}} a_{\mathrm{c}} \left(T_{\mathrm{s}} - T_{\mathrm{f}}\right) \tag{2}$$

for the solid.

Assuming zero solid velocity for a non-deforming medium Equation (2) reduces to:

$$(1-\phi) C_{\mathrm{s}} \frac{\partial T_{\mathrm{s}}(r,t)}{\partial t} = -\frac{\partial q_{\mathrm{s}}(r,t)}{\partial r} + hA_{\mathrm{p}} a_{\mathrm{c}} \left(T_{\mathrm{s}} - T_{\mathrm{f}}\right) \tag{3}$$

Combining of (1) and (3) gives:

$$(1-\phi) C_s \frac{\partial T_s(r,t)}{\partial t} + \phi C_f \frac{\partial T_f(r,t)}{\partial t} = C_f U_f \frac{\partial T_f(r,t)}{\partial r} - \frac{\partial q_s(r,t)}{\partial r} \tag{4}$$

Fourier's law of heat transfer gives:

$$q = -KA \frac{\partial T}{\partial r} \tag{5}$$

Substituting in Equation (4) and noting that the condition for energy balance causes the cross sectional area of heat transfer to cancel leads to:

$$(1-\phi) C_s \frac{\partial T_s(r,t)}{\partial t} + \phi \frac{\partial T_f(r,t)}{\partial t} = C_f U_f \frac{\partial T_f(r,t)}{\partial r} + KA \frac{\partial^2 T_s}{\partial r^2} \tag{6}$$

Equation (6) sums up the energy balances for a system consisting of one fluid and the porous medium. For carbon dioxide injection an energy balance equation for the gas is required. This must be written taking into consideration individual fluid saturation evolution in the porous medium.

This is written as:

$$(1-s_{\mathrm{w}}) C_{\mathrm{CO_2}} \frac{\partial T_{\mathrm{CO_2}}(r,t)}{\partial t} + C_{\mathrm{CO_2}} U_{\mathrm{CO_2}} = C_{\mathrm{CO_2}} U_{\mathrm{CO_2}}(s_{\mathrm{w}}) \frac{\partial T_{\mathrm{CO_2}}(r,t)}{\partial r} = K \frac{\partial^2 T_{\mathrm{CO_2}}(r,t)}{\partial r^2} + hA_{\mathrm{p}} a_{\mathrm{c}} \left(T_{\mathrm{s}} - T_{\mathrm{CO_2}}\right) \tag{7}$$

In terms of saturation Equation (7) can be modified to account for water saturation in view of the two phase flow as:

$$(1-\phi) C_{\mathrm{s}} \frac{\partial T_{\mathrm{s}}(r,t)}{\partial t} + s_{\mathrm{w}} C_{\mathrm{w}} \frac{\partial T_{\mathrm{w}}(r,t)}{\partial t} = C_{\mathrm{w}} U_{\mathrm{w}} = C_{\mathrm{w}} U_{\mathrm{w}}(s_{\mathrm{w}}) \frac{\partial T_{\mathrm{w}}(r,t)}{\partial r} + K \frac{\partial^2 T_{\mathrm{s}}}{\partial r^2} \tag{8}$$

Equations (7) and (8) are consistent with the fact that individual phase flow or velocities are functions of saturation which in this case is the wetting phase saturation.

Adding Equations (7) and (8) gives:

$$(1-\phi) C_{\mathrm{s}} \frac{\partial T_{\mathrm{s}}(r,t)}{\partial t} + s_{\mathrm{w}} C_{\mathrm{w}} \frac{\partial T_{\mathrm{w}}(r,t)}{\partial t} + (1-s_{\mathrm{w}}) C_{\mathrm{CO_2}} \frac{\partial T_{\mathrm{CO_2}}(r,t)}{\partial t} + C_{\mathrm{w}} U_{\mathrm{w}}(s_{\mathrm{w}}) \frac{\partial T_{\mathrm{w}}(r,t)}{\partial r} + C_{\mathrm{CO_2}} U_{\mathrm{CO_2}}(s_{\mathrm{w}}) \frac{\partial T_{\mathrm{CO_2}}}{\partial r} = K \frac{\partial^2 T_{\mathrm{s}}}{\partial r^2} + K \frac{\partial^2 T_{\mathrm{CO_2}}}{\partial r^2} + hA_{\mathrm{p}} a_{\mathrm{c}} \left(T_{\mathrm{s}} - T_{\mathrm{CO_2}}\right) \tag{9}$$

By adopting the local thermal equilibrium concept the following is applicable:

$$T_{\mathrm{s}} = T_{\mathrm{w}} = T_{\mathrm{CO_2}} \tag{10}$$

Substituting the condition expressed by Equation (9) into Equation (10) and adopting the temperature of the solid grains as that of the system temperature gives the resulting energy balance equation as:

$$(1-\phi) C_{\mathrm{s}} \frac{\partial T_{\mathrm{s}}(r,t)}{\partial t} + s_{\mathrm{w}} C_{\mathrm{w}} \frac{\partial T_{\mathrm{s}}(r,t)}{\partial t} + (1-s_{\mathrm{w}}) C_{\mathrm{CO_2}} \frac{\partial T_{\mathrm{s}}(r,t)}{\partial t} + C_{\mathrm{w}} U_{\mathrm{w}}(s_{\mathrm{w}}) \frac{\partial T_{\mathrm{s}}(r,t)}{\partial r} + C_{\mathrm{CO_2}} U_{\mathrm{CO_2}}(s_{\mathrm{w}}) \frac{\partial T_{\mathrm{s}}}{\partial r} = K \frac{\partial^2 T_{\mathrm{s}}}{\partial r^2} + K \frac{\partial^2 T_{\mathrm{s}}}{\partial r^2} + hA_p a_c \left(T_{s-} T_s\right) \tag{11}$$

This equation can finally be written as:

$$\left[\left(1-\phi\right)C_{\mathrm{s}}+s_{\mathrm{w}}C_{\mathrm{w}}+\left(1-s_{\mathrm{w}}\right)C_{\mathrm{CO_2}}\right]\frac{\partial T_{\mathrm{s}}\left(r,t\right)}{\partial t}+$$

$$\left[U_{\mathrm{w}}\left(s_{\mathrm{w}}\right)+U_{\mathrm{CO_2}}\left(s_{\mathrm{w}}\right)\right]\frac{\partial T_{\mathrm{s}}\left(r,t\right)}{\partial r}=2K\frac{\partial T^{2}{}_{\mathrm{s}}\left(r,t\right)}{\partial r^{2}} \quad (12)$$

By assuming the local thermal equilibrium concept as before, and dividing through by the coefficient of the heat accumulation term gives:

$$\frac{\partial T_{\mathrm{s}}\left(r,t\right)}{\partial t}+\frac{C_{\mathrm{w}}U_{\mathrm{w}}\left(s_{\mathrm{w}}\right)+C_{\mathrm{w}}U_{\mathrm{CO_2}}\left(s_{\mathrm{w}}\right)}{\left[\left(1-\phi\right)C_{\mathrm{s}}+s_{\mathrm{w}}C_{\mathrm{w}}+\left(1-s_{\mathrm{w}}\right)C_{\mathrm{CO_2}}\right]}\frac{\partial T_{\mathrm{s}}\left(r,t\right)}{\partial r}$$

$$=\frac{2K}{\left[\left(1-\phi\right)C_{\mathrm{s}}+s_{\mathrm{w}}C_{\mathrm{w}}+\left(1-s_{\mathrm{w}}\right)C_{\mathrm{CO_2}}\right]}\frac{\partial T^{2}{}_{\mathrm{s}}\left(r,t\right)}{\partial r^{2}} \quad (13)$$

So far the heat balance equations contain the volumetric heat capacities denoted by C_{i} where *i* denote a phase. This is calculated as:

$$C_{\mathrm{i}}=c_{\mathrm{p}}\rho_{\mathrm{i}} \quad (14)$$

are volumetric heat capacity of a phase, specific heat capacity of a phase and density of a phase respectively. Substituting Equation (14) into Equation (13) gives:

$$\frac{\partial T_{\mathrm{s}}\left(r,t\right)}{\partial t}+$$

$$\frac{C_{\mathrm{w}}U_{\mathrm{w}}\left(s_{\mathrm{w}}\right)+C_{\mathrm{CO_2}}U_{\mathrm{CO_2}}\left(s_{\mathrm{w}}\right)}{\left[\left(1-\phi\right)c_{\mathrm{p_s}}\rho_{\mathrm{s}}+s_{\mathrm{w}}c_{\mathrm{p_w}}\rho_{\mathrm{w}}+\left(1-s_{\mathrm{w}}\right)c_{\mathrm{p}\,\mathrm{CO_2}}\rho_{\mathrm{CO_2}}\right]}\frac{\partial T_{\mathrm{s}}\left(r,t\right)}{\partial r}$$

$$=\frac{2K}{\left[\left(1-\phi\right)c_{\mathrm{s}}\rho_{\mathrm{s}}+s_{\mathrm{w}}c_{\mathrm{w}}\rho_{\mathrm{w}}+\left(1-s_{\mathrm{w}}\right)c_{\mathrm{p}\,\mathrm{CO_2}}\rho_{\mathrm{CO_2}}\right]}\frac{\partial T^{2}{}_{\mathrm{s}}\left(r,t\right)}{\partial r^{2}} \quad (15)$$

The classical heat diffusion equation in cylindrical coordinate for heat and mass transfer scenarios is written as:

$$\frac{\partial T\left(r,t\right)}{\partial t}+\frac{C_{\mathrm{f}}U}{\left(1-\phi\right)c_{\mathrm{p}}\rho_{\mathrm{s}}}\frac{\partial T\left(r,t\right)}{\partial r}=\alpha_{\mathrm{th}}\frac{\partial^{2}T}{\partial r^{2}} \quad (16)$$

Comparison of coefficients in Equations (15) and (16) shows the following:

$$\frac{CU}{\left(1-\phi\right)c_{\mathrm{p}}\rho}\equiv\frac{U_{\mathrm{CO_2}}\left(s_{\mathrm{w}}\right)+U_{\mathrm{w}}\left(S_{\mathrm{w}}\right)}{\left[\left(1-\phi\right)c_{\mathrm{p_s}}\rho_{\mathrm{s}}+s_{\mathrm{w}}c_{\mathrm{p_w}}\rho_{\mathrm{w}}+\left(1-s_{\mathrm{w}}\right)c_{\mathrm{p}\,\mathrm{CO_2}}\rho_{\mathrm{CO_2}}\right]} \quad (17)$$

$$\alpha_{\mathrm{th}}\equiv\frac{2K}{\left[\left(1-\phi\right)c_{\mathrm{s}}\rho_{\mathrm{s}}+s_{\mathrm{w}}c_{\mathrm{w}}\rho_{\mathrm{w}}+\left(1-s_{\mathrm{w}}\right)c_{\mathrm{p}\,\mathrm{CO_2}}\rho_{\mathrm{CO_2}}\right]}$$

In Equation (17) the expression for the thermal diffusivity of the system is an affective one and it is saturation dependent. Accordingly the thermal conductivity, K, in the numerator is an effective one and equally saturation dependent and can be computed using mixing rules.

Two Phase Flow Heat Transfer Analysis

In the light of two phase flow in a saline aquifer involving the injection of supercritical carbon dioxide the relative strength of diffusion to convective heat transfer can be obtained by writing consideration fluid saturation evolution in the system during injection. In this regard the following can be written:

$$\frac{\left(c\rho\right)_{\mathrm{CO_2}}\left(S_{\mathrm{w}}\right)U_{\mathrm{CO_2}}\left(s_{\mathrm{w}}\right)+\left(c\rho\right)_{\mathrm{w}}U_{\mathrm{w}}\left(S_{\mathrm{w}}\right)}{h_{\mathrm{th}}}dT\equiv$$

$$\frac{c_{\mathrm{p}\,\mathrm{CO_2}}\rho_{CO_2}\left(1-S_{\mathrm{w}}\right)\left(\phi\right)+c_{\mathrm{w}}\rho_{\mathrm{w}}S_{\mathrm{w}}\left(\phi\right)+c_{\mathrm{S}}\rho_{\mathrm{s}}\left(1-\phi\right)}{t_{\mathrm{con}}}dT \quad (18)$$

The convective time scale is given by:

$$t_{\mathrm{con}}\equiv\frac{c_{\mathrm{p}\,\mathrm{CO_2}}\rho_{\mathrm{CO_2}}\left(1-S_{\mathrm{w}}\right)\left(\phi\right)+c_{\mathrm{w}}\rho_{\mathrm{w}}S_{\mathrm{w}}\left(\phi\right)+c_{\mathrm{S}}\rho_{\mathrm{s}}\left(1-\phi\right)}{c_{\mathrm{CO_2}}\rho_{\mathrm{CO_2}}\left(1-S_{\mathrm{w}}\right)\phi U_{\mathrm{CO_2}}\left(S_{\mathrm{w}}\right)+c_{\mathrm{w}}\rho_{\mathrm{w}}S_{\mathrm{w}}\phi U_{\mathrm{w}}\left(S_{\mathrm{w}}\right)}h_{\mathrm{th}} \quad (19)$$

The effective thermal diffusivity is given by:

$$\alpha_{\mathrm{th}}=\frac{2K}{\left[\left(1-\phi\right)c_{\mathrm{s}}\rho_{\mathrm{s}}+s_{\mathrm{w}}c_{\mathrm{w}}\rho_{\mathrm{w}}+\left(1-s_{\mathrm{w}}\right)c_{p\,\mathrm{CO_2}}\rho_{\mathrm{CO_2}}\right]} \quad (20)$$

To calculate the effective thermal diffusivity for a two phase fluid flow that reflects the actual heat diffusion state of the system requires using mixing rule.[6] In practice this is done using different averaging techniques including arithmetic, geometric and harmonic averaging technique. However, in statistics the choice of the proper averaging techniques require taking into consideration the physical process interest. The harmonic mean, H, of the positive real numbers $x_1, x_2, \ldots, x_n > 0$ is defined by:[7]

$$H=\frac{n}{\frac{1}{x_1}+\frac{1}{x_2}+\ldots\frac{1}{x_{\mathrm{n}}}}=\frac{n}{\sum_{\mathrm{i}}^{\mathrm{n}}\frac{1}{x_{\mathrm{i}}}} \quad (21)$$

Table 1. Bulk rock thermal conductivity (W MK^{-1}) for different saturations of carbon injected carbon dioxide[6]

CO_2 saturation	Ketzin-Sandstone			Ketz-Claystone		
	arithmetic	harmonic	geometric	arithmetic	harmonic	geometric
0	6.03	2.77	1.86	1.93	1.85	1.9
0.1	6.02	1.48	4.67	1.928	1.66	1.89
0,2	6.02	1.01	4.49	1.926	1.5	1.87
0.3	6	0.77	4.32	1.924	1,37	1.86
0.4	5.99	.0.62	4.15	1.923	1.26	1.84
0.5	5.98	0.52	3.99	1.921	1.17	1.83
0,6	5.97	0.44	3.85	1.919	1.09	1.81
0.7	5.97	0.39	3.68	1.917	1.02	1.8
0.8	5.96	0.35	3.54	1.916	0.96	1.79
0.9	5.95	0.31	3.4	1.914	0.9	1.77
1	5.94	0.28	3.27	1.912	0.85	1.76

To justify the use of the harmonic averaging technique in computing the effective thermal diffusivity requires due reverence to a typical case of harmonic mean application population genetics statistical analysis. In population genetics the harmonic mean is used when calculating the effects of fluctuations in generation size on the effective breeding population. Invariably this considers the fact that a limited size of the generation is like a bottle neck and means that a very small number of individuals are contributing disproportionately to the gene pool which can result in higher levels of inbreeding.

The significance of the bottle neck concept can be appreciated by noting that the rate at which water is poured out of a bottle depends on the size of the bottle's neck. In this regard the neck of the bottle is a major contributor to the rate. For a two face flow involving the injection of carbon dioxide into a saline aquifer for storage and the resulting displacement of the resident brine the bottle neck concept applies in the sense that the effective thermal diffusivity given by Equation (20) changes with saturation and it is mostly governed by the saturation of the injected gas that is supposed to occupy the porous medium by displacing the resident fluid.

Using Equation (21) the effective thermal conductivity *K* will be calculated as:

$$K_{\text{eff}} = \frac{3}{\frac{1}{K_{CO_2}(1-S_w)} + \frac{1}{K_w S_w} + \frac{1}{K_s(1-\phi)}} =$$

$$\frac{3K_{CO_2}(1-S_w)K_w S_w K_s(1-\phi)}{K_{CO_2}(1-S_w)K_w S_w + K_w S_w K_s(1-\phi) + K_s(1-\phi)K_{CO_2}(1-S_w)} \quad (22)$$

The effective value of the product of density and heat capacity of the system is calculated similarly as:

$$(c_p\rho)_{\text{eff}} = \frac{3}{\frac{1}{c_{p_{CO_2}}\rho_{CO_2}(1-S_w)^2\phi^2} + \frac{1}{c_{p_w}\rho_w S_w^2\phi^2} + \frac{1}{c_{p_s}\rho_s(1-\phi)^2}} \quad (23)$$

The equivalent thermal diffusivity can now be written as:

$$\alpha_{\text{eff}} = 2\frac{K_{CO_2}(1-S_w)K_w S_w K_s(1-\phi)}{K_{CO_2}(1-S_w)K_w S_w + K_w S_w K_s(1-\phi) + K_s(1-\phi)K_{CO_2}} * \frac{c_{p_{CO_2}}\rho_{CO_2}(1-S_w)\phi + c_{p_w}\rho_w S_w\phi + c_{p_s}\rho_s(1-\phi)}{c_{p_{CO_2}}\rho_{CO_2}(1-S_w)\phi c_{p_w}\rho_w\phi S_w c_{p_s}\rho_s(1-\phi)} \quad (24)$$

Using mixing rule and the harmonic mean concept, Equation (24) gives the effective thermal diffusivity of the system as a function of water saturation. Equation (15) will henceforth be written as:

$$\frac{\partial T_s(r,t)}{\partial t} + \frac{c_w\rho_w S_w U_w(s_w) + c_{CO_2}\rho_{CO_2}(1-S_w)U_{CO_2}}{\left[(1-\phi)c_{p_s}\rho_s + s_w c_{p_w}\rho_w + (1-s_w)c_{p_{CO_2}}\rho_{CO_2}\right]}\frac{\partial T_s(r,t)}{\partial r} = \alpha_{\text{eff}}\frac{\partial T^2{}_s(r,t)}{\partial r^2} \quad (25)$$

An Approximation to the energy balance equation

To obtain an approximation to the energy balance equation obtained previously two physical realities will be duly exploited.

They are the relatively high hydraulic diffusivity of the system compared to the low thermal diffusivity of heat.[4]

This makes it possible to eliminate the diffusive part of the energy balance equation for the system.

The second is the decrease in effective thermal diffusivity of the system due to increase in injected gas saturation. In the light of carbon dioxide injection the effect would be to create higher gas saturations. Table 1 indicates the effect of gas saturation on bulk or effective thermal conductivity for a typical carbon geo-sequestration in a saline aquifer with an eminent decrease of this parameter with increasing gas saturation. The table shows a dramatic decrease for the case of a harmonic mean of thermal conductivity.

From Table 1 it is realized that since the concentration of gas is increasing the effective thermal conductivity of the system will be determined by gas saturation and since this decreases the ratio of this parameter to the effective volumetric heat capacity (effective value of the product of density and heat capacity for the elements of the system), a measure of effective thermal diffusivity will also decrease with gas saturation. By custom a comparison between diffusive and accumulation term gives:

$$\frac{\partial T}{t_{\text{thdif}}} \equiv \frac{\alpha_{\text{e}} \partial T}{h_{\text{th}}^2} \tag{26}$$

This equation can be rearranged as:

$$t_{\text{thdif}} \equiv \frac{h_{\text{th}}^2}{\alpha_{\text{e}}} \tag{27}$$

where

t_{thdif} and α_{e} are thermal diffusive time scale and effective diffusivity, respectively.

By Equation (27) the diffusive time scale will be given as:

$$t_{\text{diff}} = \frac{(\rho c)_{\text{e}}}{(\rho c)_{\text{f}}} \frac{1}{U_{\text{D}}} \frac{t_{\text{con}}}{h_{\text{th}}} \alpha_{\text{eff}} \tag{28}$$

Substituting for effective diffusivity gives:

$$t_{\text{diff}} = \frac{(\rho c)_{\text{e}}}{(\rho c)_{\text{f}}} \frac{1}{U_{CO_2}(S_{\text{w}}) + U_{\text{w}}(S_{\text{w}})} * \frac{t_{\text{con}}}{h_{\text{th}}} \frac{2K_{CO_2}(1-S_{\text{w}})K_{\text{w}}S_{\text{w}}K_{\text{s}}(1-\phi)}{K_{CO_2}(1-S_{\text{w}})K_{\text{w}}S_{\text{w}} + K_{\text{w}}S_{\text{w}}K_{\text{s}}(1-\phi) + K_{\text{s}}(1-\phi)K_{CO_2}} * \frac{c_{p_{CO_2}}\rho_{CO_2}(1-S_{\text{w}})\phi + c_{p_{\text{w}}}\rho_{\text{w}}S_{\text{w}}\phi + c_{p_{\text{s}}}\rho_{\text{s}}(1-\phi)}{c_{p_{CO_2}}\rho_{CO_2}(1-S_{\text{w}})\phi c_{p_{\text{w}}}\rho_{\text{w}}\phi S_{\text{w}} c_{p_{\text{s}}}\rho_{\text{s}}(1-\phi)} \tag{29}$$

Implications for Hydrodynamic Environments and Lithology

The transfer of heat between injected fluid and the solid grains of the porous medium will occur generally on a diffusive time scale given by:[7, 8]

$$t_{\text{diff}} = \frac{d_{\text{g}}^2}{\alpha} \tag{30}$$

where

t_{diff}, d_{g}, and α are diffusive time scale, average grain diameter, and thermal diffusivity of grain material, respectively.

On the other hand the time required for the injected fluid to migrate across a pore space is measure by:

$$t_{\text{con}} = \frac{d_g s \phi}{u} \tag{31}$$

where

t_{con}, s, ϕ and u are convective time scale, injected fluid saturation, average sediments porosity and Darcy velocity, respectively.

For local thermal equilibrium criterion the convective time scale must be longer than the diffusive time[8] scale and this requires an average grain diameter:

$$d_{\text{g}} \prec \frac{\alpha s \phi}{u} \tag{32}$$

This requires grains sizes in the range of 0.1 to 0.01 which is typically met by sandstone sedimentation environment. The implication is that near the injection well the zone acquires the temperature of the injected fluid while at the leading edge of the injected fluid the far field temperature of the formation persists. This leads to the creation of a transition zone.

If it is assumed that the value of thermal diffusivity is negligible and the diffusive time scale given by Equation (28) is not important then energy balance Equation (25) reduces to:

$$\frac{\partial T_{\text{s}}(r,t)}{\partial t} + \frac{c_{\text{w}}\rho_{\text{w}}S_{\text{w}}U_{\text{w}}(s_{\text{w}}) + c_{CO_2}\rho_{CO_2}(1-S_{\text{w}})U_{CO_2}}{\left[(1-\phi)c_{p_{\text{s}}}\rho_{\text{s}} + s_{\text{w}}c_{p_{\text{w}}}\rho_{\text{w}} + (1-s_{\text{w}})c_{p_{CO_2}}\rho_{CO_2}\right]} \frac{\partial T_{\text{s}}(r,t)}{\partial r} = 0 \tag{33}$$

At a given time in the flow field the total flux in the system is written as:

$$Q = U_{\text{tot}} = U_{\text{w}} + U_{\text{CO}_2} = U_{\text{CO}_2} = \frac{Kk_{\text{rwir}}}{\mu_{\text{w}}}\frac{\partial P_{\text{w}}}{\partial \text{r}} + \frac{Kk_{\text{rgiw}}}{\mu_{\text{g}}}\frac{\partial P_{\text{CO}_2}}{\partial r} \quad (34)$$

where Q = injection rate.

Consequently the following can be written for the numerator of the coefficient of the space derivative on the right hand side of Equation (33):

$$U_{\text{tot}} = U_{\text{w}} + U_{\text{CO}_2} = c_{\text{w}}\rho_{\text{w}}S_{\text{w}}U_{\text{w}}\left(S_{\text{w}}\right) + c_{\text{CO}_2}\rho_{\text{CO}_2}\left(1-S_{w}\right)U_{\text{CO}_2} \quad (35)$$

This reduces Equation (33) to the following form:

$$\frac{\partial T_{\text{s}}(r,t)}{\partial t} + \frac{c_{\text{CO}_2}\rho_{\text{CO}_2}U_{\text{tot}}}{\left[\left(1-\phi\right)c_{p_{\text{s}}}\rho_{\text{s}} + s_{\text{w}}\phi c_{p_{\text{w}}}\rho_{\text{w}} + \left(1-s_{\text{w}}\right)\phi c_{p_{\text{CO}_2}}\rho_{\text{CO}_2}\right]}\frac{\partial T_{\text{s}}(r,t)}{\partial r} = 0 \quad (36)$$

Flow Velocity Field

The final equation for energy balance of the injected fluid must contain the appropriate form of the convective thermal energy transfer term. To be able to obtain this requires deducing the velocity field for the system. The following assumptions are considered pertinent:

1. The high differential thermal expansion mismatch between the fluids and the solid grains if the rock will cause the solid to resist the expansion of the fluids

2. The low thermal expansivity of the grains will cause small expansion of the grains

3. From assumptions 1 and 2 the resulting volume change due to temperature changes will be negligible

4. The effective compressibility of the system is negligible

On the basis of the above assumptions the flow rate of the injected fluid (gas) is calculated as:

$$Q = \frac{dV}{dt} \quad (37)$$

Q, dV, dt are injection rate, volume flow and time interval, respectively in the flow field.

The relationship between fluid volume at a given radial distance, the wellbore radius, the thickness of the aquifer and porosity of the aquifer is given by:

$$V = \pi r^2 h\phi - \pi r_{\text{w}}^2 h\phi = \pi h\phi\left(r^2 - r_{\text{w}}^2\right) \quad (38)$$

where V, r_{w}, r, h are volume flow, well radius, radial distance and thickness of aquifer, respectively.

The change in volume is given by:

$$\partial V = \pi r^2 h\phi - \pi r_{\text{w}}^2 h\phi = \partial\pi h\phi\left(r^2 - r_{\text{w}}^2\right) = 2\pi r\phi h\partial r \quad (39)$$

Substituting for volume change in Equation (39) into Equation (37) gives:

$$Q = \frac{\partial V}{\partial t} = 2\pi rh\phi\frac{\partial r}{\partial t} \quad (40)$$

The change of radial distance with time is gas flow velocity given by:

$$\frac{\partial r}{\partial t} = u \quad (41)$$

where μ = velocity field

Equation (40) becomes:

$$Q = \frac{\partial V}{\partial t} = 2\pi rh\phi u \quad (42)$$

Multiplying Equation (42) through by well radius and rearranging gives:

$$\frac{r_{\text{w}}Q}{\phi 2\pi r r_{\text{w}}h} = u \quad (43)$$

In Equation (43) the cross sectional area A_c opened to gas injection is given by:

$$A_{\text{c}} = 2\pi r_{\text{w}}h \quad (44)$$

Substitution of this into Equation (43) gives:

$$\frac{r_{\text{w}}U_{\text{tot}}}{\phi r} = u \quad (45)$$

where U= injection velocity

The interstitial velocity is obtained by dividing the injection velocity by the porosity of the sediment as:

$$U_{\text{int}} = \frac{U_{\text{tot}}}{\phi} \tag{46}$$

Substitution of Equation (46) into (45) gives:

$$u = \frac{r_w}{r} U_{\text{int}} \tag{47}$$

This equation shows a decrease with radial distance from the well bore. Substitution of this into the energy balance Equation (36) gives:

$$\frac{\partial T_s(r,t)}{\partial t} + \frac{c_{CO_2}\rho_{CO_2} r_w U_{\text{int}}}{\left[(1-\phi)c_{p_s}\rho_s + s_w\phi c_{p_w}\rho_w + (1-s_w)\phi c_{p_{CO_2}}\rho_{CO_2}\right]} * \frac{1}{r}\frac{\partial T_s(r,t)}{\partial r} = 0 \tag{48}$$

Equation (48) is a linear hyperbolic partial differential equation where the temperature field propagates with a velocity U_p given by:

$$U_p = \frac{c_{CO_2}\rho_{CO_2} r_w U_{\text{int}}}{\left[(1-\phi)c_{p_s}\rho_s + s_w\phi c_{p_w}\rho_w + (1-s_w)\phi c_{p_{CO_2}}\rho_{CO_2}\right] r} \tag{49}$$

The effective volumetric thermal capacity of the system is measured by the equation:

$$C_{\text{efth}} = (1-\phi)c_{p_s}\rho_s + s_{i_w}c_{p_w}\rho_w + (1-s_{iw})c_{p_{CO_2}}\rho_{CO_2} \tag{50}$$

It is customary to assume that this parameter is independent of fluids saturations.[9]

Analytical Solution

The general form of Equation (48) reads:[10]

$$u_t + b\frac{1}{r}u_r = 0 \tag{51}$$

The analytical solution using maple program command is given by:

$$u(r,t) = F\left(\frac{-r^2+2tb}{2b}\right), \quad F = F(t) \tag{52}$$

In order to obtain the function F the following boundary condition is used:

$$u(o,t) = u_{\text{inj}}) \tag{53}$$

This means that at all times of injection the temperature of the sand face at the point of injection where the radial distance is zero must be realistically equal to that of the temperature of the injection fluid.

Substituting this boundary condition into Equation (52) gives *F* as:

$$F = \frac{u_{\text{inj}}}{t} \tag{54}$$

Substituting this into Equation (52) gives:

$$u(r,t) = \frac{u_{\text{inj}}}{t}\left(\frac{-r^2+2tb}{2b}\right) = u_{\text{inj}}\left(\frac{t}{t} - \frac{r^2}{2tb}\right) \tag{55}$$

Substituting temperature for *u* gives:

$$T(r,t) = \frac{T_{\text{inj}}}{t}\left(\frac{-r^2+2tb}{2b}\right) = T_{\text{inj}}\left(1 - \frac{r^2}{2tb}\right) \tag{56}$$

The value of *b* at a given irreducible water saturation will depend on the injection rate and the interfacial tension as well as the viscosity of the injected carbon dioxide and this is given by the capillary number. Equation (56) can be written in a dimensionless form by defining the following dimensionless variables:

$$r_D = \frac{r}{r_{aq}}, \quad , T_D = \frac{T(r,t) - T_0}{T_{\text{inj}} - T_0} \tag{57}$$

where

r_D, r, r_{aq}, T_D, T_{inj} and T_0 are dimensionless radius, radial distance from sand face, dimensionless temperature, dimensionless injection temperature and initial temperature of formation, respectively.

$$t_D = \frac{q}{r_w 2\pi r_{aq} h} t \tag{58}$$

where

t_D, q, r_{aq}, h and t are dimensionless time, injection rate, radius of aquifer, thickness of aquifer and time of injection, respectively.

The final solution can be written as:

$$T_D = \frac{T_{inj}}{t}\left(\frac{-r^2+2tb}{2b}\right) = T_{inj_D}\left(1-\frac{qr_D^2}{2t_D 2\pi r_{aq} hb}\right) \quad (59)$$

The dimensionless temperature corresponding to the injection temperature is calculated as:

$$T_{inj_D} = \frac{T_{inj}(0,t)-T_0}{T_{inj}-T_0} \quad (60)$$

Consequently Equation (48) becomes:

$$\frac{\partial T_s(r,t)}{\partial t} + \frac{c_{CO_2}\rho_{CO_2} r_w U_{int}}{\left[(1-\phi)c_{p_s}\rho_s + s_w\phi c_{p_w}\rho_w + (1-s_w)\phi c_{p_{CO_2}}\rho_{CO_2}\right]}\frac{1}{r}\frac{\partial T_s(r,t)}{\partial r} = 0 \quad (61)$$

and

$$U_p = \frac{c_{CO_2}\rho_{CO_2} r_w U_{int}}{\left[(1-\phi)c_{p_s}\rho_s + c_{p_w}\rho_w + c_{p\,CO_2}\rho_{CO_2}\right]r} \quad (62)$$

The derivation of petrophysical properties evolution with temperature in the flow field requires coupled thermal and petrophysical properties dependence on temperature models. Capillary pressure, apparent water saturation and contact angle dependence on temperature are expressed by the following:[11]

$$P_{cT} = P_{rf}\left(\frac{\beta+T}{\beta+T_{rf}}\right) \quad (63)$$

$$\bar{S_w} = \left[1+\left(\alpha P_{cT}\frac{\beta_0+T_{rf}}{\beta_0+T}\right)^n\right]^{-m} \quad (64)$$

$$\cos\phi = \phi_{rf}\left(\frac{a+bT_{rf}}{a+bT}\right)\left(\frac{\beta+T}{\beta+T_{rf}}\right) \quad (65)$$

where S, P_{cT}, P_{rf}, β_0, T_{rf}, T, ϕ_{rf} and ϕ are apparent water saturation, capillary pressure at a given temperature T, reference capillary pressure, a parameter relating to temperature dependence of interfacial tension, reference temperature, temperature of interest, reference contact angle and contact angle at temperature of interest, α, n and m=1+1/n are empirical constants.

For a two phase flow of immiscible fluids in porous media McWhorter[12] and Sunada presented the following equations for the relative permeability of the wetting and non-wetting phase:

$$k_{rw} = (S_e)^{\frac{2+3\lambda}{\lambda}} \quad (66)$$

$$k_{nr} = (1-s_w)^2\left(1-S_e^{\frac{2+\lambda}{\lambda}}\right)$$

where k_{rw}, k_{nr} and λ are relative permeability of the wetting phase fluid, relative permeability of the non-wetting phase fluid and pore size distribution index, respectively.

Discussion

In view of the desire to optimize oil recovery in both secondary and tertiary recoveries schemes, a number of researches with published data have been reported on wettability and its evolution under different conditions of operations, in response to changes in reservoir rock surface energies caused by interaction between different crude oil components.[13] The objective of this analytical work is to investigate the effect of non-isothermal two phase flow on contact angle and wettability and compare these with existing findings.

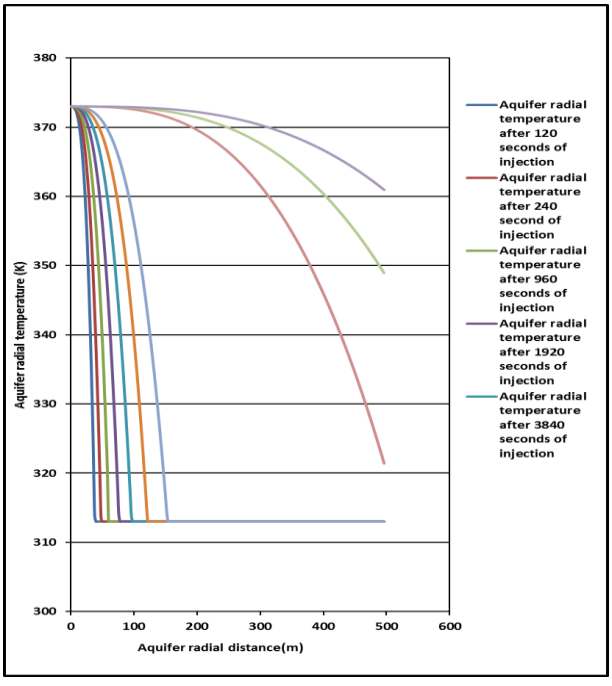

Figure 1. A plot of aquifer radial temperature profile for different times of gas injection

Consequently, to be able to better discuss the results of this analytical work in the context of reported trends in the petroleum industry there is the need to apply appropriate theories in areas related to these properties of the system.

The following text will suffice to be able to explain some of the findings of this work.

In using Equations (65) and (66) for saturation and wettability computations 0.032 % of beta reported by Hugh and Brent[11] was taken to be the representative of that of carbon dioxide water system. This is in recognition of the percentage of this gas in the air. In view of wettability being a pore scale phenomenon a positive value of this was used for contact angle computations to account for wettability increase with temperature. Figure 1 shows a plot of aquifer radial temperature for different times of injection. This plot has been generated from the solution of the final energy balance Equation (48) which is a linear hyperbolic equation characteristic of wave phenomena in mathematical physics. Accordingly, the temperature field behaves in this manner. It shows that after half a month the thermal pulse had propagated to the aquifer boundary (500 m).This, therefore, shows a gradual increase in the ambient temperature of the system.

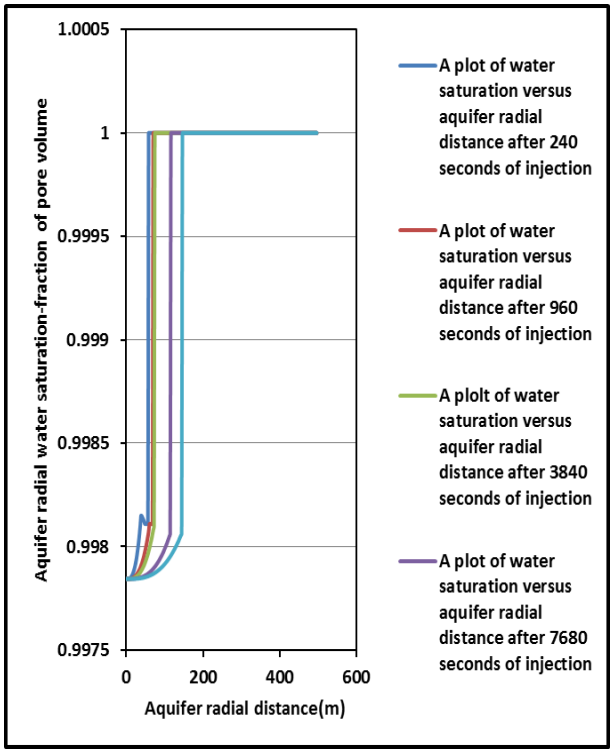

Figure 2. A plot of water saturation versus aquifer radial distance for different times of gas injection.

Figure 2 shows a plot of resident brine saturation as a function of aquifer radial distance for different times of injection. Accordingly, it shows that for longer times of injection water saturation close to the sand face or well face is lower and far away the saturation is hundred percent, meaning non invasion of injected gas.

Figure 3 shows injected gas saturation as a function of aquifer radial distance for different times of injection. It is worthy of note that one of the motivations for this paper is the desire to investigate the nature of the shock characteristic of the injected fluid the subject of which was covered by the Bucley-Leverette theory of frontal advancement.[14] In this theory application of mass balance to the injected fluid results in a parabolic partial differential equation that is characteristic of diffusive processes. However, for high injection rates typical of the flow rate used in this work the effect of capillary forces that give rise to the diffusive nature of the mass balance equation is considered negligible and the overall result is a linear hyperbolic equation that describes saturation evolution with time and space. Under such conditions there is shock described by a saturation jump to a given frontal saturation and this depends on the initial value of the irreducible saturation of the injected fluid.[15] The injection rates where relative measure of viscous to capillary forces is extremely high a typical solution for saturation versus distance as a function of time will show viscous forces to be equal to ten times capillary forces. The exihits a typical shock characteristic of high injection rate where the ratio of viscous forces to capillary forces is 10. The nature of the shock is such that different saturations behind the shock propagate with a velocity equal to the frontal velocity.

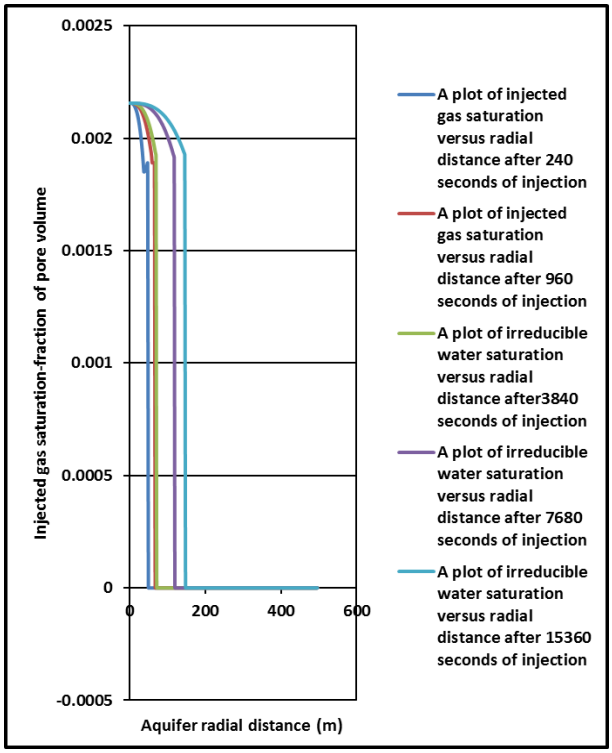

Figure 3. A plot of injected gas saturation as a function of aquifer radial distance for different times of injection.

In this zone the velocity of the shock is related to the gradient of the fractional flow versus saturation curve evaluated at the saturation of the front. Thus, in the context of this work it is expected to obtain the characteristic shock propagation in a manner that befits a temperature gradient flow. To distinguish this clearly requires applying the temperature field solution in this work. In this regard it is clear that at a given time of injection the temperature is higher near the well face and almost equal to the system ambient temperature at distances far away from the well face. It will be seen that the contact angle will decrease with increasing temperature and by applying the interstitial

dependent capillary number theory the cosine of the contact angle will be higher close to the well bore and lower far away. The effect is to decrease the ratio of viscous to capillary forces. There is, therefore, a capillary dominated flow near the well bore and decreases far away from it. The effect is to create a curvature close to the well bore for all different times of injection gas saturation profile versus radial distance. This means that as the gravity of capillary forces diminishes the shapes of the shock approaches those with high viscous effect and with ratio of viscous to capillary forces of equal to 3.

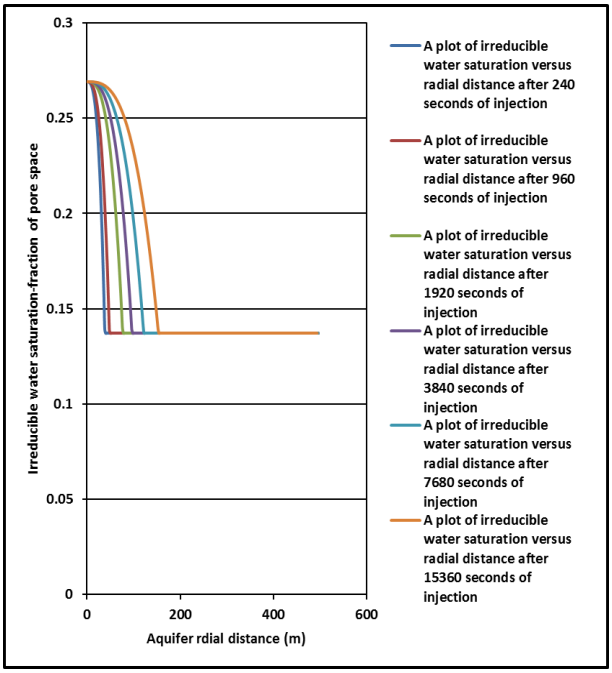

Figure 4. A plot of irreducible water saturation versus aquifer radial distance for different times of gas injection.

This explains why gas saturation profile shows a curve near the well bore and a steep shape far away and this is quite consistent with the temperature dependent capillary number as explained earlier. The capillary number is the ratio of viscous to capillary forces but this has been defined in a number of ways pertaining to the physics of the problem in question. In this problem the interstitial capillary number has been found appropriate because it uses the interstitial velocity which is the superficial velocity divided by porosityof the sediment. Its appropriateness in the context of this paper stems from the fact that wettability is pore level phenomenon and deserves to be considered in the light of interstitial flow rather than superficial flow.

Figure 4 show a plot of irreducible water saturation as a function of radial distance for different times of injection. The finding in this work is consistent with those reported by Ancilotto et. al[16] which indicated an increase in irreducible water saturation for supercritical carbon dioxide and brine system. Accordingly irreducible water saturation is higher for longer times of injection as observed in Figure 4.

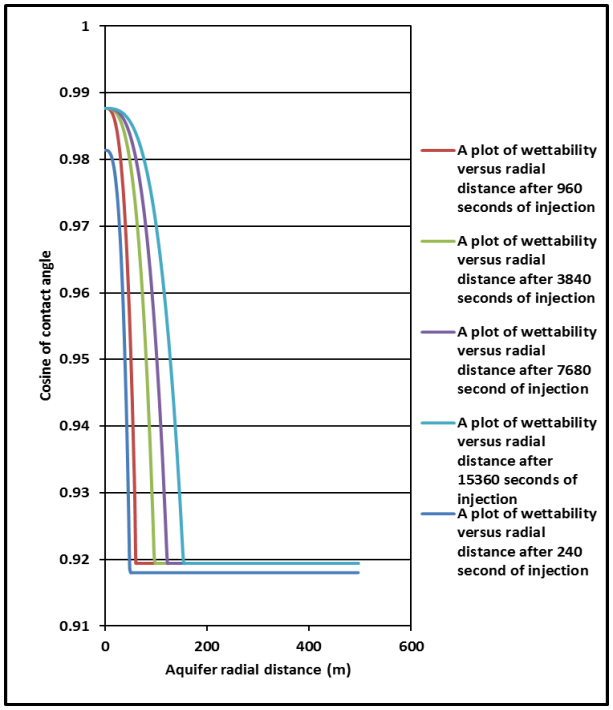

Figure 5. A plot of aquifer wettability evolution versus aquifer radial distance for different times of gas injection.

Figure 5 shows the wettability evolution of the aquifer carbon dioxide and water system under non-isothermal flow conditions. The wettability of a system is measured by the cosine of the contact angle. As explained previously, the contact angle decreases with temperature and this means an increase in the wettability of the system. The nature of the plot, however, reflects the boundary condition used for the solution of the energy balance equation. Accordingly at all times the temperature of the inlet or sand face is equal to that of the injected fluid [373 K]. Therefore, the ambient wettability jumps to that commensurate with this inlet temperature and decreases as the temperature decreases. Bikkina[17] has reported a decrease in contact angle for carbon dioxide water system for a silica surface. Schembre et.al[18] have also reported a similar trend.

Conclusion

The effect of temperature on immiscible flow in porous media has been a subject of interest in the petroleum industry due to the desire to optimise oil recovers under thermal operations involving water injection. Consequently a number of experimental data abound in wettability and contact angle measurements pertaining to oil and water systems. The area of carbon geo-sequestration is new and not much data abound in this area compared to the petroleum industry.

However, few published works exists in this area and these coupled with reported trends in contact angle obtained in different but similar areas of investigations (chemical physics) have provided a basis of comparison using analytical results from this work. In this regard the following conclusion can be drawn.

1. The effect of temperature gradient in immiscible two phase flow involving supercritical carbon dioxide and resident formation brine is to cause a curvature to be observed on the saturation shocks at regions close to the sand face and then dissipate far away from this resulting in a shock similar to those of isothermal conditions reported in the literature.

2. The effect of temperature gradient flow is to increase the wettability of the system close to the sand face and this evolves with time.

3. This analytical work has also established the positive temperature dependent nature of irreducible water saturation.

4. In the field of immiscible two-phase flow in porous media information about saturation evolution is always obtained from flow tests. This analytical work has provided a means of obtaining an idea about saturation evolution under non isothermal conditions.

Acknowledgements

The authors wish to acknowledge the support provided by Dalhousie University for computational work and Cape Breton University's Office of Research and Graduate Studies for financial support.

Greek Letters

α_{eff}= effective thermal diffusivity, $m^2 s^{-1}$

β= temperature dependence of interfacial tension, mN m^{-1}

ω= Temperature gradient of surface tension, mN K^{-1}

μ= velocity field

ϕ= contact angle, degrees

ρ= density, kg m^{-3}

References

[1]Sharer, R. J., and Traxler, L. P., *The Ancient Maya*, Stanford Univ. Press, USA. **2006**, ISBN 0804748179

[2]Hildenbrand, A., Schlomer, S., Krooss, B. M., and Littke, R., *Geofluids*, **2004**, 4, 61-80.

[3]Zimmerman, R.W., *Int. J. Rock Mechan. Mining Sci.*, **2000**, *37*, 79-87.

[4]Charlez, P. A., *Rock Mechanics, Vol. 2 -Petroleum Application*, Edition Technip, Paris, **1997**.

[5]Minkowycz, W. J., Haji-Sheikh, A., and Vafai, K., *Int. J. Heat Mass Transfer*, **1999**, *42*, 3373-3385.

[6]Hurter, S., Garnett, A., Bielinski. A, and Kopp, A., SPE Conf. Offshore Europe, September 4-7, **2007**, Aberdeen, Scotland, U.K.

[7]Chou, Y., *Statistical Analysis*, Holt, Rinehart & Winston of Canada Ltd, **1975**, 2nd edition, ISBN: 9780030894220.

[8]Rayward-Smith, W. J., and Woods, A. W., *Geophys. Res. Lett.*, **2011**, *38(6)*. L06407, doi:10.1029/2010GL046412.

[9]Prats, M., *J. Petroleum Techn.*, **1969**, *1(3)*, 323-332.

[10]Strikwerda, J. C., *Finite Difference Schemes and Partial Differential Equations*, Soc. Ind. Appl. Math., USA, **2004.** ISBN: 978-0-89871-567-5

[11]Hugh Y. S., and Brent, E. S., *Water Resources Res.*, **1998,** *34(10)*, 2587-2597.

[12]McWhorter, D. B and Sunada, D. K., *Water Resources Res.*, **1990**, *26(3)*, 339-413.

[13]Dixit, A. B., McDougall, S. R., Sorbie, K. S., and Buckley, J. S., *SPE/DOE Improved Oil Recovery Symp*., April 1-24, **1996,** Tulsa, Oklahoma.

[14]Yortsos, Y. C., and Fokas, A. S., *SPE J.* **1983**, *23(1)*, 115-124.

[15]Smith, C. R., Tracy, G. W., and Farrar, R. L., *Applied Reservoir Engineering*, Oil and Gas Consult. Int. (OGCI), **1992**, Tulsa, USA: paper by Ahmed A. Gawish, *"The Compensation Study of Viscosity and Volume Changes in Natural Gases"*.

[16]Ancilotto, F., Faccin, F., and Toigo, F., *Phys. Rev. B*, **2000,** *62*. 17035-17042.

[17]Bikkina, P. K., *Int. J. Greenhouse Gas Control*, **2011**, *5(5)*, 1259–1271.

[18]Schembre, J. M., Tang, G.-Q., and Kovscek, A. R., *SPE Res. Eval. Eng*, **2006**, *9(3)*, 239-250. SPE-93831-PA.

Received: 11.09.2015.
Accepted: 10.02.2016.